HHS Public Access

Author manuscript

Cell Rep. Author manuscript; available in PMC 2023 August 04.

Published in final edited form as:

Cell Rep. 2023 May 30; 42(5): 112436. doi:10.1016/j.celrep.2023.112436.

PSGL-1 attenuates early TCR signaling to suppress CD8+ T cell progenitor differentiation and elicit terminal CD8+ T cell exhaustion

Jennifer L. Hope[1,2], **Dennis C. Otero**[1,2], **Eun-Ah Bae**[1,2], **Christopher J. Stairiker**[1,2], **Ashley B. Palete**[1,2], **Hannah A. Faso**[1,2], **Michelle Lin**[1,2], **Monique L. Henriquez**[1,2], **Sreeja Roy**[1,2], **Hyungseok Seo**[3], **Xue Lei**[4], **Eric S. Wang**[5], **Savio Chow**[4], **Roberto Tinoco**[1,2], **Gregory A. Daniels**[6], **Kevin Yip**[4], **Alexandre Rosa Campos**[7], **Jun Yin**[8], **Peter D. Adams**[4], **Anjana Rao**[3], **Linda M. Bradley**[1,2,9,*]

[1]Cancer Metabolism and Microenvironment, NCI-Designated Cancer Center, Sanford Burnham Prebys Medical Discovery Institute, La Jolla, CA 92037, USA

[2]Immunity and Pathogenesis Program, Sanford Burnham Prebys Medical Discovery Institute, La Jolla, CA 92037, USA

[3]Division of Signaling and Gene Expression, La Jolla Institute for Immunology, La Jolla, CA 92037, USA

[4]Cancer Genome and Epigenetics, NCI-Designated Cancer Center, Sanford Burnham Prebys Medical Discovery Institute, La Jolla, CA 92037, USA

[5]Cancer Molecular Therapeutics, NCI-Designated Cancer Center, Sanford Burnham Prebys Medical Discovery Institute, La Jolla, CA 92037, USA

[6]Department of Medicine, Moores Cancer Center at UC San Diego Health, La Jolla, CA 92037, USA

[7]Proteomics Core, Sanford Burnham Prebys Medical Discovery Institute, La Jolla, CA 92037, USA

[8]Bioinformatics Core, Sanford Burnham Prebys Medical Discovery Institute, La Jolla, CA 92037, USA

[9]Lead contact

*Correspondence: lbradley@sbpdiscovery.org.

AUTHOR CONTRIBUTIONS

Conceptualization, J.L.H., D.C.O., and L.M.B.; methodology, J.L.H., D.C.O., H.S., X.L., A.R.C., E.S.W., K.Y., J.Y., P.D.A., A.R., and L.M.B.; investigation, J.L.H., D.C.O., C.J.S., E.-A.B., A.B.P., H.A.F., M.L., M.L.H., S.R., R.T., H.S., A.R.C., S.C., J.Y., X.L., and E.S.W.; resources, G.A.D.; writing, J.L.H. and L.M.B.

DECLARATION OF INTERESTS

L.M.B. and R.T. hold patents for PSGL-1 modulators and uses thereof (US10858436B2, WO2016007653A3). L.M.B. and J.L.H. hold patents for PSGL-1 antagonists and uses thereof (63/481570).

INCLUSION AND DIVERSITY

We support inclusive, diverse, and equitable conduct of research. One or more of the authors of this paper received support from a program designed to increase minority representation in their field of research.

SUPPLEMENTAL INFORMATION

Supplemental information can be found online at https://doi.org/10.1016/j.celrep.2023.112436.

SUMMARY

PSGL-1 (P-selectin glycoprotein-1) is a T cell-intrinsic checkpoint regulator of exhaustion with an unknown mechanism of action. Here, we show that PSGL-1 acts upstream of PD-1 and requires co-ligation with the T cell receptor (TCR) to attenuate activation of mouse and human $CD8^+$ T cells and drive terminal T cell exhaustion. PSGL-1 directly restrains TCR signaling via Zap70 and maintains expression of the Zap70 inhibitor Sts-1. PSGL-1 deficiency empowers $CD8^+$ T cells to respond to low-affinity TCR ligands and inhibit growth of PD-1-blockade-resistant melanoma by enabling tumor-infiltrating T cells to sustain an elevated metabolic gene signature supportive of increased glycolysis and glucose uptake to promote effector function. This outcome is coupled to an increased abundance of $CD8^+$ T cell stem cell-like progenitors that maintain effector functions. Additionally, pharmacologic blockade of PSGL-1 curtails T cell exhaustion, indicating that PSGL-1 represents an immunotherapeutic target for PD-1-blockade-resistant tumors.

In brief

In this study, Hope et al. reveal intrinsic mechanisms through which the cell surface molecule PSGL-1 (P-selectin glycoprotein-1) modulates T cell responses and drives differentiation to terminal exhaustion in chronic virus infection and melanoma. Their study highlights the targetability of PSGL-1 as an emerging immune checkpoint blockade strategy.

Graphical abstract

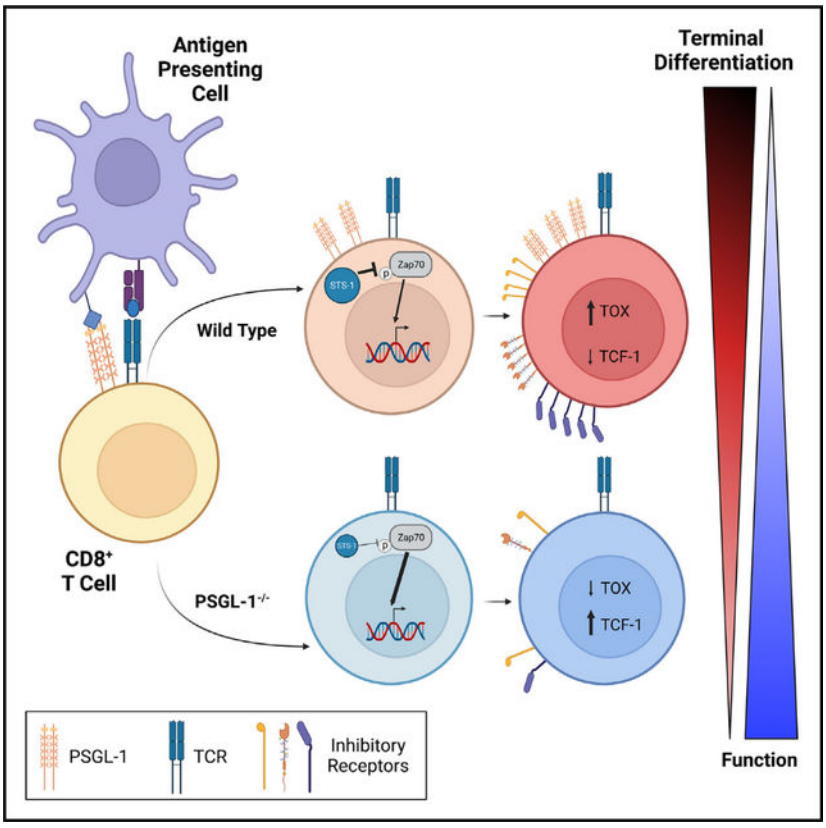

INTRODUCTION

CD8$^+$ effector T cells (T_{EFF}) are vital in protecting against and clearing virally infected cells and tumor cells. However, in settings of chronic viral infection and cancer, multiple factors including sustained antigen exposure promote T cell exhaustion. Accompanied by progressive decline in effector functions and proliferative capacity, this state is linked to increased co-expression of multiple inhibitory receptors including PD-1, CTLA-4, LAG3, and TIM-3.[1] The discovery of immune checkpoint blockade (ICB) monoclonal antibody therapy to promote anti-tumor immunity by inhibiting CTLA-4 and/or PD-1 on T cells is one of most significant cancer therapeutic breakthroughs of the last decade, with efficacy shown across many cancers.[2] Despite dramatic success in some patients, a significant population fails to respond to ICB. It is therefore essential to identify novel mechanisms regulating the differentiation of exhausted T cells (T_{EX}) that could expand ICB's applicability to more patients. In particular, it will be critical to develop ICB strategies that support the development and maintenance of stem cell-like (T_{SC}) or progenitor T_{EX} (T_{PEX}) that retain the capacity for proliferation and T_{EFF} function.[3]

PSGL-1 (P-selectin glycoprotein ligand-1) is expressed on most hematopoietic cells, including T cells.[4,5] We identified that genetic deletion of PSGL-1 prevented development of T_{EX} and supported viral clearance in the chronic lymphocytic choriomeningitis virus (LCMV) clone 13 (Cl13) model[6] due to increased T_{EFF} function that was accompanied by decreased inhibitory receptor expression. PSGL-1 deficiency also supported growth control of a PD-1-blockade-resistant melanoma tumor.[6] Furthermore, PSGL-1 deficiency with acute LCMV Armstrong infection promoted greater T_{EFF} and memory progenitor T cell formation,[7] underscoring the fundamental role PSGL-1 plays as a regulator of T cell responses. In this study, we investigated cellular and molecular mechanisms by which PSGL-1 signaling intrinsically regulates T_{EX} differentiation including the impact of PSGL-1 on T cell receptor (TCR) signaling, glycolysis, and the promotion of T_{SC} and T_{PEX}. We demonstrate herein that PSGL-1 ligation concomitant with TCR ligation drives T_{EX} differentiation in human and mouse CD8$^+$ T cells. Critically, we show that blockade of PSGL-1 recapitulates PSGL-1 deficiency in antitumor and antiviral responses, and its distinct mechanism of T cell inhibition underscores the translational potential of targeting PSGL-1 by ICB.

RESULTS

PSGL-1 restrains TCR signaling magnitude and duration

Since PSGL-1 deficiency enhanced T_{EFF} responses, we addressed whether PSGL-1 modulates CD8$^+$ T cell responses to TCR engagement. TCR stimulation of naive wild-type (WT) and PSGL-1$^{-/-}$ OT-I CD8$^+$ T cells showed that PSGL-1 deficiency enabled higher expression of the T cell activation markers CD25, CD69, CD44, and PD-1 (Figure 1A)[8–11] and greater functionality (Figure S1A). To directly evaluate TCR signaling, we assessed phosphorylation of Zap70, Erk1/2, and Akt by western blot (Figure 1B) and found greater activation of each of these signaling molecules in PSGL-1$^{-/-}$ T cells (Figure S1B), with the greatest effect on pAkt levels in PSGL-1$^{-/-}$ compared with WT T cells (Figure 1C),

demonstrating that PSGL-1 expression inherently limits T cell activation from the time of initial TCR engagement.

To address intrinsic TCR signaling regulation by PSGL-1 under conditions of T cell exhaustion, we used an *in vitro* model[12] comparing OT-I *in vitro* T_{EFF} (iT_{EFF}) with OT-I *in vitro* T_{EX} (iT_{EX}). Since PSGL-1 deficiency enabled responsiveness to lower levels of TCR stimulation, we hypothesized that PSGL-1 deficiency may increase TCR sensitivity to lower-affinity ligands. iT_{EX} and rested iT_{EFF} were generated with the SIINFEKL ovalbumin $(OVA)_{(257–264)}$ peptide (N4) or with the lower OT-I TCR affinity variants[13] SIIQFEKL (Q4), SIITFEKL (T4), or SIIVFEKL (V4), and we evaluated early $CD8^+$ T cell activation by assessing CD69,[8] CD25,[14] and CD44[11] expression. 18 h after peptide stimulation (Figure 2A), similar levels of CD69 were observed between WT and PSGL-$1^{-/-}$ OT-I cells activated by N4, Q4, and T4, while significantly more CD69 was observed in PSGL-$1^{-/-}$ OT-I cells activated by V4. Significantly more CD25 and CD44 were observed in PSGL-$1^{-/-}$ OT-I cells under all conditions (Figures 2B and 2C).

We also assessed T cell function in WT and PSGL-$1^{-/-}$ OT-I iT_{EFF} and iT_{EX} generated with the N4 or Q4 peptides (Figure 2C). WT and PSGL-$1^{-/-}$ iT_{EFF} generated with either peptide had comparable frequencies of interferon γ (IFNγ) and tumor necrosis factor α (TNF-α) cytokine-producing cells, and most were double producers. As expected, WT iT_{EX} generated with these peptides were highly exhausted, with few cytokine producers (Figures 2D and 2E). However, PSGL-$1^{-/-}$ iT_{EX} elicited with N4 showed increased co-production of IFNγ and TNF-α (4.2-fold) (Figures 2D and 2E) compared with WT iT_{EX}, with fewer non-cytokine-producing cells overall (Figure 2F). Notably, PSGL-$1^{-/-}$ $CD8^+$ T cells induced with the lower affinity Q4 retained an increased capacity for cytokine co-production (Figures 2D and 2F) with a 3.8-fold increase over WT iT_{EX}. These results show that PSGL-1 restrains early T cell activation. Further, with iT_{EX} conditions, PSGL-1 limits responses to lower levels of TCR signals and lower-affinity antigens, which would be detrimental to T cell responses, particularly in the context of lower-affinity tumor cell antigens.

To further interrogate PSGL-1-mediated regulation of TCR signaling, we performed total and phospho-proteomics analysis of naive and stimulated WT and PSGL-$1^{-/-}$ OT-I cells. Relative expression levels of 7,014 total and 9,294 phosphorylated proteins were evaluated. After activation, 576 phosphorylated proteins were significantly differentially expressed between WT and PSGL-$1^{-/-}$ OT-I cells (Figure S2A). Pathway analysis identified 22 significantly enriched pathways, including “T cell receptor signaling” (Figure S2B). Phosphorylation of several proteins associated with regulation of T cell signaling was significantly upregulated in PSGL-$1^{-/-}$ T cells (Figure S2C). Also notable were changes in proteins regulating proliferation and survival (Figure S2D), calcium signaling, and metabolism (Figure S2E). Gene set enrichment analysis confirmed greater activation of the ERK1/2 pathway in PSGL-$1^{-/-}$ OT-I cells (Figure S2F). These data indicate that PSGL-1 signals play a critical role in regulating the T cell response to TCR engagement. Importantly, few changes were observed in total protein expression in naive WT cells compared with naive PSGL-$1^{-/-}$ cells (30 up, 14 down). Of the 576 differentially expressed phosphoproteins, only 127 were similarly differentially expressed in naive cells.

Previous studies of T cells showed that PSGL-1, a large, glycosylated protein, migrates to the uropod that forms at the back of cells during polarized movement.[15] PSGL-1 was therefore hypothesized to be outside the region of TCR/peptide contact. To address the spatial relationship of the TCR complex and PSGL-1, we analyzed their distribution by microscopy. Without crosslinking of TCR (CD3) or PSGL-1, both molecules were evenly distributed over the cell (Figure 3A). Upon TCR ligation, CD3 formed punctate staining indicative of clustering and co-clustered with PSGL-1. However, upon ligation with anti-PSGL-1 alone, PSGL-1 clustered to one side of the T cell, while CD3 remained dispersed. When both CD3 and PSGL-1 were ligated simultaneously, they co-localized and migrated to one region of the cell. Co-localization of CD3 and PSGL-1 on primary $CD8^+$ T cells was quantified by analysis of 10,000 $CD8^+$ T cells via imaging flow cytometry. This approach confirmed that co-localization of CD3 and PSGL-1 was greatest following co-ligation of both molecules (Figures S3A–S3C; similarity score, 2.4 ± 0.3 median absolute deviation [MAD]), showing that PSGL-1 is optimally positioned to directly regulate TCR signals, particularly when PSGL-1 is concomitantly engaged.

We previously analyzed $GP_{(33–41)}$ LCMV Cl13 virus-specific $CD8^+$ T cells from WT and PSGL-$1^{-/-}$ mice by RNA sequencing (RNA-seq) 8 days post infection (dpi).[6] Reanalysis of these data identified the significant downregulation of the gene *Ubash3b* (3.25-fold change, $p \leq 0.05$) in PSGL-$1^{-/-}$ T cells (GEO: GSE80113). *Ubash3b* encodes the protein Sts-1 (suppressor of T cell signaling-1), a phosphatase shown to be a potent negative regulator of TCR signaling by inhibiting Zap70.[16,17] *Ubash3b* expression is increased in $CD8^+$ T_{EFF} compared with naive cells (ImmGen RNA-seq dataset), suggesting that Sts-1 levels may limit the extent of T cell activation to prevent hyperresponsiveness.[16] What regulates Sts-1 expression in T cells has yet to be established. Since PSGL-$1^{-/-}$ $CD8^+$ T cells demonstrated increased TCR signaling, we hypothesized that the epigenetic landscape would reflect this enhanced state of activation. ATAC-seq (assay for transposase-accessible chromatin sequencing) tracings identified an enhancer region within *Ubash3b* with significantly less open chromatin in PSGL-$1^{-/-}$ T cells compared with WT T cells after TCR stimulation (Figures 3B and S3D–S3G). Protein analysis confirmed that naive and activated PSGL-$1^{-/-}$ OT-I T cells express less Sts-1 (Figures 3C and S3H). Imaging flow cytometry identified a high correlation in localization of Sts-1 and Zap70 in naive and activated WT and PSGL-$1^{-/-}$ $CD8^+$ T cells, as well as between PSGL-1 and Zap70 (Figures 3D and 3E). Together, these data suggest that greater availability and activation of Zap70 (pZap70) may be in part due to decreased levels of Sts-1 leading to enhanced TCR signaling in PSGL-$1^{-/-}$ $CD8^+$ T cells.

PSGL-1 restrains glycolysis in $CD8^+$ T cells

Given the inhibitory effects of PSGL-1 on $CD8^+$ T cell activation, we addressed its impact on glycolytic metabolism, which underlies T_{EFF} development after TCR engagement.[18] Using the Seahorse Glycolytic Rate Assay, glycolysis was assessed in WT or PSGL-$1^{-/-}$ OT-I T cells after activation for 3 days (Figures 4A and 4B). Both baseline and maximal glycolysis levels were significantly elevated in PSGL-$1^{-/-}$ T cells. Thus, we hypothesized that PSGL-$1^{-/-}$ $CD8^+$ T cells retain glycolytic activity under exhaustion conditions. To test this, we assessed glycolysis in *in vitro*-generated PSGL-$1^{-/-}$ and WT OT-I iT_{EX}.

As expected, exhausted WT OT-I iT_{EX} have low levels of extracellular acidification rate (ECAR) and oxygen consumption rate (OCR) at baseline and upon mitochondrial uncoupling (Figure 4C). Comparatively, PSGL-$1^{-/-}$ OT-I iT_{EX} retained high levels of ECAR and OCR (Figure 4C), corresponding to higher levels of proton efflux rate (PER) and glycolic PER (glycoPER) than WT OT-I iT_{EX} (Figure 4D). The results show that PSGL-$1^{-/-}$ $CD8^+$ T cells remain more glycolytically active under conditions of chronic TCR stimulation.

We confirmed that increased glycolysis of PSGL-$1^{-/-}$ $CD8^+$ T cells was accompanied by greater glucose utilization by quantifying 2-NBD glucose analog (2-NBDG) uptake by WT and PSGL-$1^{-/-}$ OT-I cells after stimulation with $OVA_{257–264}$ (Figures 4E and 4F). No differences in glucose uptake by naive WT or PSGL-$1^{-/-}$ OT-I cells were observed. We reported that PSGL-$1^{-/-}$ mice exhibit significant control of the PD-1-blockade-resistant YUMM1.5 melanoma tumor line,[6] which does not express PSGL-1 (Figure S4). To assess whether differences in glucose uptake could contribute to an enhanced anti-tumor response, we assessed 2-NBDG uptake by activated ($CD44^{hi}$) $CD8^+$ T cells from YUMM1.5-bearing mice. In $CD44^{hi}$ $CD8^+$ T cells from YUMM1.5 tumors, spleens, and tumor draining lymph nodes (DLNs) assessed immediately *ex vivo*, we observed significantly greater glucose uptake by PSGL-$1^{-/-}$ $CD8^+$ T cells compared with WT $CD8^+$ T cells (Figure 4G). The data show that PSGL-$1^{-/-}$ $CD8^+$ tumor-infiltrating lymphocytes (TILs) maintain a greater capacity for glucose uptake and enhanced glycolytic capabilities under exhaustive conditions.

scRNA-seq reveals an enhanced metabolic state of PSGL-1-deficient $CD8^+$ TILs

Adoptively transferred PSGL-$1^{-/-}$ OT-I cells enable greater control of B16-OVA melanoma in mice than WT OT-I cells.[6] To assess intrinsic transcriptional differences between WT and PSGL-$1^{-/-}$ T cells *in vivo*, we used single-cell RNA-seq (scRNA-seq) and the B16-OVA model with adoptive transfer of WT or PSGL-$1^{-/-}$ OT-I cells (Figure S5A). To account for an uneven capture rate, data were down-sampled to an equal number of cells for analysis. Unbiased clustering of donor OT-I cells revealed a high level of overlap between WT and PSGL-$1^{-/-}$ OT-I cells (Figures 5A–5C). We identified genes that were globally differentially expressed in PSGL-$1^{-/-}$ cells (e.g., *Rpl35*, *Tmsb10*) as well as cluster-specific gene alterations (e.g., *Hist1h2ap*, *H2afv*, *Malat1*) (Figure S5B). Overall, more PSGL-$1^{-/-}$ OT-I $CD8^+$ T cells expressed genes associated with $CD8^+$ T_{EFF} (*Ifng*, *Gzma*, *Gzmb*, *Gzmc*, *Tbx21*) compared with WT cells (Figure S5C). We evaluated T cell functionality on a per-cluster basis (Figure S5D). Overall, more PSGL-$1^{-/-}$ OT-I cells expressed *Ifng* across the clusters, with significantly greater levels in clusters 0, 1, 2, and 4. Differences in *GzmA* were found in clusters 3, 4, and 5, while *Gzmb* expression was largely comparable across all clusters. Using SeqGeq to “gate” and evaluate gene expression within subsets, we identified OT-I cells co-expressing granzyme B (*Gzmb*) and IFNγ (*Ifng*). In PSGL-$1^{-/-}$ OT-I cells, co-expression of *Gzmb* and *Ifng* was linked to greater expression of *Mtor* and *Hif1a* as well as engagement in cell cycle (*Mki67*) but without changes in cell survival (*Bcl2*) (Figure 5D).

As we identified greater glycolytic capacity with PSGL-1 deficiency in OT-I cells, we assessed expression of genes that regulate glycolysis in WT and PSGL-$1^{-/-}$ OT-I cells

by overlaying gene expression on a SeqGeq-generated t-distributed stochastic neighbor embedding (tSNE) plot (Figure 5E). Individual *Ifng* and *Gzmb* expression was largely localized in PSGL-$1^{-/-}$ OT-I T cell clusters. Furthermore, greater expression of the genes *Pgam1*, *Aldoa*, *Eno1*, and *Ldha*, which regulate glycolysis, was co-localized with these T_{EFF} PSGL-$1^{-/-}$ OT-I T cells. These analyses underscore that PSGL-1 deficiency confers greater glycolytic capacity in the tumor microenvironment (TME) and that this greater metabolic capacity is linked to greater T_{EFF} function. Thus, PSGL-1 deficiency releases metabolic constraints that are essential for efficient $CD8^+$ T cell effector function in the TME.

PSGL-1 suppresses persistence of T_{SC}/T_{PEX}

Many studies have now defined that T_{SC} with a capacity for self-renewal, expansion, and development of effector function express the transcription factor TCF-1.[19–21] In metastatic melanoma, TCF-1^+CD8^+ T cells from patient tumors are associated with objective responses to PD-1 blockade.[22] Conversely, the transcription factor TOX is a fundamental regulator of a T cell's fate of irreversible exhaustion.[23–26] However, co-expression of TOX and TCF-1 can distinguish less terminally differentiated T_{EX} that retain effector function.[24,26] To address if enhanced functionality of PSGL-$1^{-/-}$ $CD8^+$ T cells was a result of altered differentiation, we assessed TCF-1 and TOX expression in WT and PSGL-$1^{-/-}$ $GP_{(33–41)}{}^+$ virus-specific T cells from spleens at 15 dpi (Figures 6A and 6B), when the virus is cleared from the sera of PSGL-$1^{-/-}$ mice.[6] TCF-1^+ cells were increased in PSGL-$1^{-/-}$ mice compared with WT mice; conversely, a large fraction of WT T cells expressed TOX compared with PSGL-$1^{-/-}$ T cells. In virus-specific $GP_{(33–41)}{}^+$ and $NP_{(396–404)}{}^+$ T cells in the blood at 9 dpi of WT and PSGL-$1^{-/-}$ mice when the virus loads are comparable, the frequencies of TCF-1^+ cells were indistinguishable; the majority of virus-specific $CD8^+$ T cells lacked expression of both TCF-1 and TOX (Figure S6A). However, dramatically fewer $GP_{(33–41)}{}^+$ T cells from PSGL-$1^{-/-}$ mice expressed TOX (Figure 6C). At 15 dpi, the phenotype of $GP_{(33–41)}{}^+$ T cells from PSGL-$1^{-/-}$ mice showed a moderate increase in TCF-1^+ cells but a drastic decrease in TOX^+ cells (Figure 6C).

Differential interleukin-7 receptor α (IL-7Rα) and KLRG-1 expression by $CD8^+$ T cells classically delineates short-lived effector cells (SLECs) and memory precursor cells (MPECs),[27] and LCMV Arm infection skews $GP_{(33–41)}$-specific PSGL-$1^{-/-}$ $CD8^+$ T cells toward the MPEC phenotype.[7] Previous studies have demonstrated an inverse relationship between TOX and KLRG-1 expression during LCMV Cl13 infection.[28] We observed that all KLRG-1^+ cells were within the TOX^- population for both WT and PSGL-$1^{-/-}$ $GP_{(33–41)}{}^+$ T cells. In $TOX^-GP_{(33–41)}{}^+$ T cells, there were fewer IL-$7Rα^-$/KLRG-1^- cells in PSGL-$1^{-/-}$ $CD8^+$ T cells and an increased representation of the IL-$7Rα^+$/KLRG-1^- and IL-$7Rα^+$/KLRG-1^+ populations (Figures S6A and S6B), further indicating decreased exhaustion.

Unlike $GP_{(33–41)}{}^+$ T cells, which persist throughout LCMV Cl13 infection, $CD8^+$ T cells recognizing the higher avidity epitope $NP_{(396–404)}$ are deleted,[29,30] yet these cells are retained in PSGL-$1^{-/-}$ mice.[6] Within $NP_{(396–404)}{}^+$ T cells, fewer PSGL-$1^{-/-}$ T cells expressed TOX at both 9 and 15 dpi, whereas fewer PSGL-$1^{-/-}$ T cells expressed only TCF-1 at 9 dpi (Figure 6C). While expression levels of TCF-1 were indistinguishable for $GP_{(33–41)}{}^+$ or $NP_{(396–401)}{}^+$ T cells, TOX expression levels were consistently lower in

PSGL-1$^{-/-}$ virus-specific T cells (Figure 6D). These data indicate that PSGL-1 deficiency prevents terminal differentiation of T_{EX} in part by limiting the expression of TOX. To confirm that this is a cell-intrinsic effect, we performed co-transfer experiments. At 60 dpi with LCMV Cl13, the frequencies of WT and PSGL-1$^{-/-}$ P14 CD8^{+} T cells were comparable, yet more PSGL-1$^{-/-}$ P14 CD8^{+} T cells displayed Slamf6 (which is highly co-expressed with TCF-1 on T_{PEX}[31]) and IL-7Rα (Figure 6E). Evaluation of TCF-1 and TOX expression in co-transferred donor P14 cells revealed that more PSGL-1$^{-/-}$ P14 CD8^{+} T cells were single positive (SP) for TCF-1 as well as double positive (DP) for TCF-1 and TOX compared with WT P14 CD8^{+} T cells (Figures 6F and 6G). Conversely, more WT P14 CD8^{+} T cells expressed TOX only (Figures 6F and 6G). Taken together, these data demonstrate that PSGL-1 signaling intrinsically regulates CD8^{+} T cell differentiation in response to repeated antigen exposure.

To assess whether PSGL-1 engagement is a driver of TOX and T_{EX} differentiation, we assessed TCF-1 and TOX expression in virus-specific $GP_{(33–41)}^{+}$ T cells from LCMV Cl13-infected WT mice following PSGL-1 agonist antibody treatment. PSGL-1 ligation reduced the expression of TCF-1 by 25%, while TOX expression was increased by 50% (Figure 6H). To address T cell intrinsic effects of PSGL-1 regulation on TCF-1 and TOX expression in response to melanoma, we analyzed adoptively transferred activated WT and PSGL-1$^{-/-}$ OT-I cells in B16-OVA tumor-bearing WT mice. The frequencies of TCF-1^{+}CD44^{+}OT-I^{+} T cells was modestly increased with intrinsic PSGL-1 deficiency (Figure 6I, left panels). In the tumor DLN, essentially all donor OT-I cells were TCF-1^{+}, but fewer cells co-expressed TOX in PSGL-1$^{-/-}$ OT-I cells (Figure 6I, right panels). Evaluation of TCF-1 and TOX showed that PSGL-1$^{-/-}$ OT-I TILs displayed a modest increase in TCF-1^{+} SP cells but decreased TOX^{+} SP cells and increased TCF-1/TOX DP cells (Figure 6J). These data show that PSGL-1 deficiency restrains the progressive differentiation toward terminal exhaustion by infiltrating tumor-specific T_{EX}.

As adoptive transfer of a sufficient number of activated PSGL-1$^{-/-}$ OT-I CD8^{+} T cells can significantly reduce tumor growth,[6] we performed adoptive co-transfers with doses of OT-I cells that are unable to inhibit B16-OVA to assess the intrinsic ability of PSGL-1 to impact T cell differentiation in the same TME. Unlike in single-transfer experiments, PD-1 and TIM-3 co-expression on donor OT-I CD8^{+} T cells was largely equivalent in a co-transfer setting (Figure S6C). 7 days after donor cell injection, there was no significant difference in the frequency of TCF-1-expressing OT-I CD8^{+} T cells, while there was a trend toward decreased frequency of TOX-expressing cells in PSGL-1$^{-/-}$ OT-I CD8^{+} T cells (Figure S6D). However, the overall expression of TOX on a per-cell basis was significantly decreased in PSGL-1$^{-/-}$ T cells compared with WT T cells in the same animals (Figure S6E). As differential TCF-1 and TOX expression in murine CD8^{+} T cells can denote cells that are the least and most terminally differentiated, we sought to identify cells that have recently differentiated from progenitors. Thus, we evaluated expression of the chemokine receptor CX3CR1, which distinguishes highly functional effector CD8^{+} T cells differentiated from TCF-1^{+} progenitor cells.[32] Significantly more PSGL-1$^{-/-}$ OT-I cells expressed CX3CR1 (Figures S6F and S6G) and also expressed more CX3CR1 on a per-cell basis (mean fluorescence intensity [MFI]) (Figure S6H), indicating less differentiation of the PSGL-1$^{-/-}$ OT-I cells toward terminal exhaustion when in the same TME. As decreased TOX expression consistently distinguished

PSGL-1$^{-/-}$ T cells in the settings of melanoma and chronic antigen stimulation, while PSGL-1 ligation enhanced TOX expression, our data confirm a fundamental and intrinsic role for PSGL-1 in regulating T_{EX} differentiation.

PSGL-1 signaling promotes exhaustion in human CD8$^+$ T cells

As PSGL-1 promotes T_{EX} differentiation, we hypothesized that PSGL-1 expression would be increased on CD8$^+$ T cells from patients with melanoma similarly to PD-1 or CTLA-4 expression. PSGL-1 (CD162) expression and cytokine production were evaluated with stimulated CD8$^+$ T cells from healthy donors and from patients with melanoma. Patient CD8$^+$ T cells, which demonstrated increased PD-1/TIM-3 expression and decreased cytokine production (Figures S7A and S7B), showed a 2.5-fold increase in PSGL-1 expression (Figures 7A and 7B). Of note, increased PSGL-1 expression was observed on all activated CD8$^+$ T cells, which may be reflective of "bystander" CD8$^+$ T cell activation, a form of antigen-independent T cell activation previously observed in some virus infections and cancers.[33] As previous studies have reported systemic inflammation in patients with metastatic melanoma,[34] the level of PSGL-1 expression on patient CD8$^+$ T cells may correlate with systemic inflammation and/or responses to immunostimulatory treatments.

Given that PSGL-1 ligation promotes CD8$^+$ T cell exhaustion during LCMV Cl13 infection and increased YUMM1.5 tumor growth, we addressed whether PSGL-1 similarly regulates human CD8$^+$ T cells by establishing an *in vitro* model of human T_{EFF} and T_{EX} differentiation from healthy donor peripheral blood mononuclear cells (PBMCs) using single (iT_{EFF}) or repeated (iT_{EX}) TCR stimulation. These conditions generate polyfunctional IFNγ- and TNF-α-producing iT_{EFF} and iT_{EX} that fail to produce cytokines upon restimulation. Restimulation of iT_{EFF} after 9 days of culture resulted in CD45RO$^+$CD8$^+$ T cells with a robust capacity to individually produce and co-produce IFNγ and TNF-α (Figures 7C and 7D), while iT_{EX} failed to produce significant amounts of either cytokine (Figures 7C and 7D).

Terminally exhausted T_{EX} express lower levels of T-bet and increased levels of Eomes (compared with T_{EFF}) in chronic LCMV Cl13 infection,[35] in patients with HIV,[36] and in the context of cancer.[37] In our *in vitro* model, relative Eomes/T-bet expression increased in iT_{EX} compared with iT_{EFF} (Figure 7E). Combined with decreased function, our results indicate that these *in-vitro*-generated cells have a phenotype reflective of T_{EX} from patients. This is particularly relevant for human T cells, as TOX expression is not limited to T_{EX}.[38] To address how PSGL-1 signaling in human T cells may contribute to CD8$^+$ T cell differentiation, iT_{EX} were cultured in the presence of a PSGL-1 agonist antibody. In 4 out of 5 donors assessed, one-time activation of T cells and addition of anti-PSGL-1 resulted in the decreased ability of these cells to produce and co-produce IFNγ and TNF-α (Figures 7C and 7D). For donors in which cytokine production dropped, capacity for co-production was ~55% of the effector cells (Figure 7D, bottom). Consistent with an incomplete differentiation of iT_{EX} from iT_{EFF} due to PSGL-1 ligation, we observed a modest increase in the relative Eomes/T-bet expression ratio (Figure 7E). When combined with repeated TCR stimulation, the Eomes/T-bet expression ratio of iT_{EX}-treated CD8$^+$ T cells increased to a similar level as iT_{EFF} without PSGL-1 ligation (Figure 7E). These

data indicate that signaling via PSGL-1 concomitant with TCR stimulation can intrinsically orchestrate the development of T_{EX} from T_{EFF} in human $CD8^+$ T cells.

Therapeutic PSGL-1 blockade limits T cell exhaustion and promotes tumor control

To evaluate whether the impact of PSGL-1 deficiency extended to cancers beyond melanoma, we tested AE17 mesothelioma tumor growth in WT vs. PSGL-$1^{-/-}$ mice. Like YUMM1.5, AE17 tumors are resistant to ICB treatment.[39] PSGL-$1^{-/-}$ mice demonstrated significantly increased control of AE17 tumors (Figure 7F), suggesting the potential for PSGL-1 as a pan-cancer ICB target. We therefore tested therapeutic blockade of PSGL-1. As the available anti-PSGL-1 antibody (Clone 4RA10) acts as an agonist, we reasoned that this may occur via crosslinking via Fc receptor binding on APCs. Thus, monovalent F(ab)s were generated and used to treat LCMV Cl13-infected mice. At 30 dpi, treatment with F(ab) antibodies did not influence the frequency of $NP_{(396–404)}{}^+$ $CD8^+$ T cells (Figure S7C) but did increase the frequency of cytokine-producing $NP_{(396–401)}$-specific (Figure S7D) and $GP_{(33–41)}$-specific (Figure S7E) $CD8^+$ T cells 8 dpi. Additionally, co-expression of the inhibitory receptors PD-1, LAG3, and TIM-3 was decreased in the 4RA10 F(ab)-treated group (Figures S7F and S7G).

Since F(ab)s have a limited half-life, which could account for the modest effects on T cell exhaustion, we generated a recombinant PSGL-1 with human immunoglobulin G1 (IgG1) Fc (rPSGL-1 Fc) and evaluated virus-specific $CD8^+$ T cell responses in LCMV Cl13-infected mice treated with rPSGL-1 Fc or control recombinant human IgG1 Fc (rIgG Fc). Although the frequencies of $NP_{(396–404)}{}^+$ T cells in the spleens were comparable between rIgG Fc- and rPSGL-1 Fc-treated mice, PD-1^+ and TIM-3^+ DP cells were significantly diminished after rPSGL-1 Fc treatment (Figure 7G). Further, overall co-expression of inhibitory receptors was reduced, consistent with reduced levels of exhaustion (3 inhibitory receptors: 80.3% vs. 64.5%) (Figure 7H). Similar results were observed when WT (CD45.2^+) mice that received WT P14 (CD45.1^+) $CD8^+$ T cells were treated with rPSGL-1 Fc, as well as decreased TOX expression (Figure S7H) and increased IFNγ production (Figure S7I).

Finally, to evaluate whether PSGL-1 blockade using rPSGL-1 Fc could promote T cell responses to cancer, we evaluated YUMM1.5 tumor growth in mice administered rPSGL-1 Fc or rIgG Fc control at the time of tumor cell inoculation (Figures 7I and 7J) or after tumor growth was established 14 days later (Figure 7K). Treatment with rPSGL-1 Fc at the time of tumor cell injection resulted in significantly reduced tumor growth that was comparable to that achieved in PSGL-1 deficient mice,[6] and T cell infiltration assessed by anti-CD3 staining indicated that rPSGL-1 treatment enhanced the infiltration and/or expansion of T cells within the tumors (Figures 7I and 7J). With established tumors, we found that PSGL-1 blockade reduced tumor growth (Figure 7K), demonstrating the feasibility of achieving inhibition of PSGL-1 signaling at a time when the growth of PD-1 ICB-resistant cancers is uncontrolled.

DISCUSSION

Here, we investigated mechanisms contributing to the function of PSGL-1 as an intrinsic T cell checkpoint inhibitor that we now show acts upstream of PD-1. We demonstrate

that PSGL-1 engagement limits responses to TCR signaling that promote T cell activation and T_{EFF} development by inhibiting proximal TCR signaling. Importantly, this was demonstrated in the absence of CD28 co-stimulation. As PD-1 blockade requires CD28 co-stimulation to reinvigorate $CD8^+$ T cells,[40] PSGL-1 blockade therefore represents a potential mechanism to restore exhausted $CD8^+$ T cells in patients non-responsive to PD-1 ICB. Notably, PSGL-1 inhibits T cell activation to low levels of TCR stimulation and low-affinity TCR ligands, indicating that PSGL-1 is a fundamental regulator that plays an essential role in preventing excessive T cell responses. Our finding that Sts-1 is diminished but not absent in PSGL-$1^{-/-}$ T cells suggests that although TCR signaling is enhanced, terminal T cell differentiation is curtailed, supporting greater development of T_{SC} and progenitors with T_{EFF} capacity under conditions of repeated antigen stimulation that otherwise promote T_{EX} development. Our results, which show greater Zap70 activation and enhanced downstream T cell signaling in the absence of PSGL-1, demonstrate that these events support effector functions, which rely upon enhanced glycolytic metabolism and glucose uptake. Further, single-cell analyses of TILs demonstrate that metabolic reprogramming in PSGL-1-deficient T cells enhances the gene expression of multiple enzymes that regulate glycolysis. These results demonstrate that PSGL-1-dependent regulation of TCR signal strength constrains CD8 T cell metabolic activity to limit antitumor responses, providing a mechanism by which PSGL-1 acts as an immune checkpoint inhibitor.

Our data show that PSGL-1 is a regulator of terminal T_{EX} differentiation and that, in its absence, $CD8^+$ T cells can retain stemness as well as T_{EFF} responses in the context of chronic antigen stimulation. In contrast, PD-1 deletion enhances T_{EFF} functions at the expense of stemness.[41] In the B16-OVA model, most PSGL-$1^{-/-}$ T cells were DP for TCF-1 and TOX, whereas with LCMV Cl13, the vast majority of PSGL-$1^{-/-}$ T cells were TOX^-. It is likely that the extent of T cell responses varies in these different models due to differences in inflammation and the strength of TCR engagement, but in all of these settings, PSGL-1 deficiency curtailed terminal T_{EX} differentiation. Our studies also demonstrate that although ligation of PSGL-1 promotes T cell exhaustion and high expression of inhibitory receptors, PSGL-1 does not directly regulate PD-1 expression. Instead, our results support a conclusion that promoting increased responses to low-level TCR engagement or low-affinity ligands is the fundamental mechanism by which PSGL-1 deficiency curtails exhaustion.

A key outstanding question regarding PSGL-1 signaling and T cell differentiation is the ligand driving T cell exhaustion. Like early studies of the PD-1/PD-L1 pathway using PD-1[42] or PD-L1 deficiency[43] that highlighted the potential for PD-1 blockade to inhibit T cell exhaustion,[44] our studies of PSGL-1-deficient $CD8^+$ T cells reveal that its underlying mechanisms of TCR inhibition could be subverted by ICB of this receptor. Although administration of rPSGL-1 *in vivo* had profound effects on limiting the development of T cell exhaustion with LCMV Cl13 infection and promoted enhanced YUMM1.5 melanoma tumor control, *in vitro* addition of rPSGL-1 to T cell culture assays did not limit T cell exhaustion. This may reflect the lack of (or insufficient) ligand expression (e.g., on another immune cell or tumor cell not included in the culture) or additional factors that support binding (e.g., pH selectiveness[45]). It is also possible that rPSGL-1 employs additional mechanisms or requires specialized niche microenvironments[46] to reduce $CD8^+$ T cell exhaustion, which will require further investigation.

Although we previously excluded selectin binding to PSGL-1 as a significant contributor to T cell exhaustion in LCMV Cl13,[6] we have not performed these studies in tumor models. We have similarly excluded the chemokines CCL19 and CCL21 as relevant ligands in the LCMV Cl13 model.[6] Moreover, their interaction with PSGL-1 is inhibited by the anti-PSGL-1 monoclonal antibody (mAb) 4RA10,[47] whereas chemokine-mediated chemotaxis is not ablated by PSGL-1-deficiency or by 4RA10 blockade[47] and therefore is unlikely to be a major driver of T cell exhaustion in tumors. The more recently identified PSGL-1 ligand, VISTA, may be of greater relevance in the context of T cell responses and differentiation in tumors. VISTA (B7H5, also called PD-1H) is an inhibitory receptor with high homology to PD-L1[48] and, independently of PSGL-1, has been identified as a novel target for modulating T cell responses and tolerance.[49] However, although VISTA$^{-/-}$ mice are resistant to some tumor models in a CD4^{+} T cell-dependent manner,[50] VISTA blockade therapy in preclinical models has largely shown efficacy only in immunotherapy combination approaches.[51] Current studies have so far shown PSGL-1 binding of VISTA in a pH-dependent manner (pH < 6.2) only *in vitro*, and binding *in vivo* has yet to be confirmed. Our ongoing studies seek to confirm if VISTA-mediated signaling through PSGL-1 drives T cell exhaustion *in vivo* in the context of cancer and if other yet-to-be-identified ligands contribute to T cell exhaustion through PSGL-1 binding.

Critically, our blocking studies in the LCMV Cl13 and YUMM1.5 models validate that ICB can recapitulate many aspects of PSGL-1 deficiency and can limit exhaustion in a therapeutic setting with delayed treatment when tumors are established. Our study also suggests a role for the development of PSGL-1-blocking therapies across many types of cancer. Further studies will be required to determine whether PSGL-1 blockade affects the responses of other PSGL-1-expressing cells in our models. Importantly, we show elevated PSGL-1 expression on melanoma patient T cells and that agonism of PSGL-1 signaling in the context of repeated TCR stimulation intrinsically promotes exhaustion in both human and mouse T cell responses. Our results highlight that a key, highly conserved function of PSGL-1 is that of a negative regulator of T cell responses and suggest that targeting PSGL-1 could enhance the potential of achieving more sustained antitumor T cell responses.

Limitations of the study

Our study primarily uses a model of genetic PSGL-1 deficiency. As such, there is the potential for developmental alterations in PSGL-1$^{-/-}$ CD8^{+} T cells that contribute to the phenotype observed. Since the recombinant PSGL-1 protein that we developed promotes enhanced T cell responses and limits T cell exhaustion in chronic LCMV infection and models of melanoma tumors, interfering with PSGL-1 signaling is sufficient to alter T cell differentiation. However, we did not find that addition of recombinant PSGL-1 protein to *in vitro* T cell assays impacts T cell responses. Future studies investigating how recombinant PSGL-1 effectively limits T cell exhaustion will provide further insight into the *in vivo* interactions of PSGL-1 expressed on T cells with potential ligands.

STAR★METHODS

RESOURCE AVAILABILITY

Lead contact—Further information and requests for resources and reagents should be directed to and will be fulfilled by the lead contact, Linda Bradley (lbradley@sbpdiscovery.org).

Materials availability—There are restrictions to the availability of recombinant PSGL-1 protein due to a pending patent. There are licensing restrictions for PSGL-$1^{-/-}$ mice crossed to transgenic lines.

Data and code availability

- Single-cell RNA-seq data (GSE226523) and ATAC-seq data (GSE226521) have been deposited at GEO and are publicly available as of the date of publication. Accession numbers are listed in the key resources table. Original western blot images, proteomics data, microscopy data, and flow cytometry data reported in this paper will be shared by the lead contact upon request. This paper analyzes existing, publicly available data (GSE80113, GSE89036). These accession numbers for the datasets are listed in the key resources table. Any additional information required to reanalyze the data reported in this paper is available from the lead contact upon request.
- This paper does not report original code.
- Any additional information required to reanalyze the data reported in this paper is available from the lead contact upon request.

EXPERIMENTAL MODEL AND SUBJECT DETAILS

Animals

Mice: C57BL/6J, B6.Cg-*Selplg*^{tm1Fur}/J (PSGL-$1^{-/-}$), C57BL/6 Tg(TcraTcrb)1100Mjb/J (OT-I), and B6.Cg-*Tcra*^{tm1Mom}Tg(TcrLCMV)327Sdz/TacMmjax (P14) were obtained from the Jackson Laboratory. Wild type OT-I and P14 mice were backcrossed to the CD45.1 background (B6.SJL-*Ptprc*^{a}*Pepc*^{b}/BoyJ). PSGL-$1^{-/-}$ were backcrossed to the Thy1.1 background (B6.PL-*Thy1*^{a}/CyJ), and further crossed with OT-I mice or P14 mice to establish these lines with PSGL-1 deficiency. All mice were kept in a barrier facility (certified by the Association for the Assessment and Accreditation of Laboratory Animal Care) on acidic water at Sanford Burnham Prebys Medical Discovery Research Institute. After LCMV infection, mice are maintained in BSL2 containment. All lines in the Bradley mouse colony are backcrossed to parental C57BL/6J or B6.PL-*Thy1*^{a}/CyJ lines annually. This study was carried out in accordance with the recommendations and approval of the Institutional Animal Care and Use Committee (IACUC).

Infection and tumor studies: For tumor initiation, 6–8-week-old male or female mice were anesthetized with 2.5% isoflurane gas, their hind flank was shaved, and tumor cells (resuspended in Matrigel (Corning):1X PBS at a 1:1 ratio) were injected subcutaneously (s.c.) in a volume of 100 μL PBS. For B16-OVA experiments, mice received 1×10^{6} B16-

OVA tumor cells. For YUMM1.5 experiments, mice received 5×10^4 YUMM1.5 tumor cells. For adoptive cell transfers, recipient mice received a tail vein injection of T cells in a volume of 100 μL PBS as indicated for the individual experiments. When naïve T cells were transferred, cells were first mixed 1:10 with C57BL/6 splenocytes obtained from uninfected/non-tumor-bearing wildtype mice. For co-transfer studies with LCMV Cl13, mice received 5×10^4 each of naïve WT ($CD45.1^+$) and PSGL-$1^{-/-}$ ($CD90.1^+$) $CD8^+$ T cells prior to LCMV Cl13 infection. For experiments where T cells were activated prior to transfer, naïve WT ($CD45.1^+$) or PSGL-$1^{-/-}$ ($CD90.1^+$) OT-I $CD8^+$ T cells were activated with immobilized anti-CD3ε (145–2C11, BioXcell) and anti-CD28 (37.51, BioXcell)(5 μg/mL, each) for 3 days prior to transfer. 1×10^6 activated WT or PSGL-$1^{-/-}$ OT-I $CD8^+$ T cells were then injected I.V. into tumor-bearing C57BL/6 ($CD45.2^+$/$CD90.2^+$) mice. For co-transfer studies with B16-OVA, B16-OVA tumor bearing mice received 5×10^5 each of activated WT ($CD45.1^+$) and PSGL-$1^{-/-}$ ($CD90.1^+$) $CD8^+$ T cells on day 14. Tumor growth was assessed three times per week by an investigator blinded to the experiment hypothesis. For YUMM1.5 studies, only male mice were used due to the presence of male antigen on the YUMM1.5 tumors. At the indicated time points, tumors, spleens, and inguinal draining and non-draining lymph nodes were collected. For LCMV Clone 13 infection, 6–8-week-old male and female mice received an intravenous injection of 2.5×10^6 FFU in a final volume of 100 μL PBS. At the indicated time points, spleens were collected.

PSGL-1 signaling inhibition treatment: (A) Anti-PSGL-1 F(ab) antibody treatment. Commercially available anti-PSGL-1 antibody (4RA10, BioXCell) and control rat IgG were enzymatically digested into F(ab) and purified by Ab Lab (University of Vancouver, British Columbia). C57BL/6 mice infected with LCMV Cl13 were treated with 100 μg of rat IgG F(ab) (control F(ab)) or anti-PSGL-1 F(ab) via intraperitoneal (I.P.) injection twice (AM and PM) on days 4, 6, 8, 10, and 12 of virus infection. (B) Recombinant PSGL-1 treatment. For LCMV Cl13 infection studies: C57BL/6 mice infected with LCMV Cl13 were treated with 100 μg of recombinant human Fc protein (control Fc) or recombinant PSGL-1-human Fc protein (rPSGL-1 Fc) via intraperitoneal (I.P.) injection on days 0, 3, and 6 of infection. For YUMM1.5 melanoma studies: YUMM1.5-tumor bearing C57BL/6 mice were treated with 100 μg of recombinant human Fc protein (control Fc) or recombinant PSGL-1-human Fc protein (rPSGL-1 Fc) via I.P. 3x/week beginning at the indicated time (day 0 or day 14).

Tissue processing: Tumors were processed using the Miltenyi Mouse Tumor Dissociation Kit and gentleMACS C tubes (Miltenyi) according to manufacturer's instructions, except with the intentional exclusion of enzyme R (due to cleavage of PSGL-1 and CD44). Spleens and lymph nodes were processed into single-cell suspensions by manual dissociation through a 70μM filter (Falcon) using a cell strainer pestle (CELLTREAT). Tumors, spleens, and lymph nodes were processed and maintained in RPMI 1640 (Corning) supplemented with 5% FBS, 1% Penicillin/Streptomycin/L-glutathione. Tumors and spleens were treated with RBC lysis buffer (0.145 M NH_4Cl, 0.05 M Tris-HCl, pH 7.2) for ~1 minute at room temperature.

Human subjects—All human PBMC samples were obtained in line with the Declaration of Helsinki principles and with prior Institutional Review Board approval. Cryopreserved

healthy donor PBMCs were purchased from iXCells Biotechnology (San Diego) and stored in liquid nitrogen until use. Melanoma patient samples were obtained in association with the UCSD Moores Cancer Center under the UCSD Moores Cancer Center Biorepository IRB (protocol number 090401). All participants provided written informed consent before the study. Patient samples were deidentified and no clinical data beyond diagnosis of melanoma was provided, ensuring the confidentiality of the subject's protected health information. Peripheral blood was obtained via venipuncture into a sodium heparin coated vacutainer (BD Green Top). PBMCs were isolated using SepMate PBMC Isolation Tubes (StemCell Technologies, Vancouver, CA) pre-filled with 15 mL of Lymphoprep (StemCell) and following manufacturer's instruction. Isolated PBMCs were cryopreserved in liquid nitrogen until use.

Viruses

LCMV C13 propagation: LCMV Cl13 virus was propagated using BHK-21 cells. BHK-21 cells were maintained in DMEM supplemented with 10% FBS, 1% Penicillin/Streptamycin (Gibco), 1% L-glutamine (Gibco), and 5% tryptose phosphate broth (Gibco). BHK-21 cells were infected with a MOI of 0.01 of LCMV Cl13 virus stocks (kind gift of Juan Carlos de la Torres) and gently rocked for 1 hour before removal of virus and replacement of media. After 48 hours of virus propagation, viral supernatant was collected, aliquoted and stored. Quantification of virus stocks was completed using the focus forming assay and Vero cells.

Cell lines

Tissue culture: YUMM1.5 tumor cells were confirmed to lack PSGL-1 expression by qRT-PCR and Western blot analysis. The YUMM1.5 melanoma tumor cell line (male) were cultured in Iscove's Modified DMEM (IMEM) supplemented with 10% fetal bovine serum (FBS), 10^5 I.U. Penicillin, 10^5 μg/mL Streptomycin, and 292 mg L-glutamine (Corning Cellgro). B16-OVA melanoma tumor cells (female) were cultured in DMEM supplemented with 10% fetal bovine serum (FBS, Corning), 10^5 I.U. Penicillin, 10^5 μg/mL Streptomycin, 292 mg L-glutamine, and 2 μg/mL Geneticin. Cells were maintained *in vitro* at 37°C, 5% CO_2. For *in vivo* experiments, tumor cell aliquots from the same passage were thawed one week and passaged 3 times prior to injection. For culturing of primary human and mouse T cells and TK-1 mouse T cells, cells were cultured in complete T cell media: RPMI 1640 supplemented with 10% FBS, 10^5 I.U. Penicillin (Gibco), 10^5 μg/mL Streptomycin (Gibco), [10 mM] HEPES buffer (Gibco), [1 mM] Sodium Pyruvate (Gibco), 1X MEM nonessential amino acids (Gibco), and [0.55 mM] betamercaptoethanol (Gibco). Cell lines were not authenticated.

Primary cell cultures

Naïve T cell enrichment: For all experiments in which isolated $CD8^+$ T cells were used, untouched naïve ($CD44^-CD62L^+$) $CD8^+$ T cells were enriched via negative selection using biotinylated antibodies at the concentrations indicated in Table 1 and using MojoSort Streptavidin Nanobeads (BioLegend). For total T cell enrichment, biotinylated CD4 was not included. Enrichments were completed in 1X HBSS (Ca^{2+} and Mg^{2+} free) containing 2% FBS and 1 mM EDTA at a cell concentration of 1×10^8/mL. $CD8^+$ T cells enriched in

this manner were on average >98% pure and depleted of CD44-expressing $CD8^+$ T cells. In all experiments, naïve $CD8^+$ T cells were enriched from 6–8-week-old male or female mice (depending on the experiment and matching the host recipients in the case of adoptive T cell transfers).

Mouse in vitro T Cell exhaustion: Cells were cultured in complete T cell media supplemented with 5 ng/mL each of recombinant murine IL-7 and IL-15 (PeproTech). One day prior to activation of OT-I cells, C57BL/6 splenocytes were made into a single-cell suspension and treated overnight with IFNγ (5 ng/mL) to induce expression of CD80 and CD86 on antigen presenting cells. Splenic OT-I and PSGL-$1^{-/-}$ OT-I $CD8^+$ T cells were isolated by negative selection with magnetic beads from uninfected female mice 8–10 weeks of age. Cells were cultured at a 1:1 ratio of $CD8^+$ T cells and IFNγ-treated splenocytes at 1×10^6/mL with either one-time stimulation with 50 ng/mL $OVA_{(257–264)}$ peptide for 48 hours (single stim), or with daily peptide stimulation with 50 ng/mL of $OVA_{(257–264)}$ peptide for 5 days (repeated stim). In experiments using SIINFEKL variant peptides, cells received either a one-time stimulation or daily peptide stimulation with 50 ng/mL of the indicated peptide. For all conditions, after 48 hours of culture, cells were washed twice and re-seeded at 0.5×10^6 cells/mL in complete T cell media. On days two and five, all conditions were harvested and the cells were counted. $CD8^+$ T cells were stained as described below (flow cytometry) to measure activation marker, inhibitory receptor, and transcription factor expression and cytokine production following restimulation with $OVA_{(257–264)}$. Additional activation analysis was performed at 18 hours. N4 = SIINFEKL, cognate peptide; Q4 = SIIQFEKL, ~18-fold decreased affinity; T4 = SIITFEKL, ~70-fold decreased affinity; V4 = SIIVFEKL, ~700-fold decreased affinity.

Human in vitro T Cell exhaustion: Cells were cultured in complete T cell media supplemented with 5 ng/mL each of recombinant human IL-7 and IL-15 (PeproTech) and 10 U/mL recombinant human IL-2. Cryopreserved healthy donor human PBMCs (purchased from iXcells Biotech) were thawed then rested for five hours at 37°C. After resting, cells were cultured at a concentration of 1×10^6 $CD3^+$ cells/mL and stimulated with 6.25 μL/mL of ImmunoCult Human CD3/CD28 T cell activator (StemCell). For PSGL-1 agonist, tissue culture plates were coated with 5 μg/mL of anti-human CD162 (KPL, Biolegend) throughout the experiment (days 0–9). On day three of activation, cells were washed and reseeded at 1×10^6 cells/mL. Cells were then divided into either iT_{EFF} or iT_{EX} conditions. iT_{EFF} conditions did not receive additional ImmunoCult after the initial 72 h; iT_{EX} conditions received an additional 6.25 μL/mL of ImmunoCult each day on days three through eight. All conditions were harvested, washed and re-seeded as above on day 6. On day 9, T cells were stained for assessment by flow cytometry as described below to measure activation marker, inhibitory receptor, and transcription factor expression and cytokine production following restimulation with ImmunoCult overnight in the presence of Brefeldin A and monensin.

METHOD DETAILS

Generation of reagents

Recombinant PSGL-1: Recombinant PSGL-1 (rPSGL-1) was generated using the pCR3 plasmid backbone and mouse PSGL-1 and human Fc sequences. rPSGL-1 was produced by

Aragen under a MTA agreement for the Bradley Lab using transient transfection of plasmid DNA into HEK 293F cells. Expressed protein in supernatants was collected and purified using single-pass chromatography, analyzed for purity and endotoxin levels, and formulated for storage in 1X PBS.

Biological assays

2-NBDG uptake assays: All solutions were prepared in glucose-free, serum-free RPMI. 2-NBDG (Cayman Chemical) uptake was performed with a 200μM solution. Cells were incubated at 37°C for 30 minutes before proceeding with staining. Cells were resuspended in FACS wash and analyzed within 30 minutes of completion of FACS staining.

T cell activation assays and signaling (mouse): Naïve $CD8^+$ T cells or total T cells ($CD4^+$ and $CD8^+$) were enriched from WT or PSGL-$1^{-/-}$ splenocytes as above. After enrichment, 1×10^6 naïve OT-I $CD8^+$ T cells were activated with immobilized anti-CD3ε (145–2C11, BioXcell) in 24-well plates at the anti-CD3ε concentration or for the time indicated. For analysis of activation status, cells were stained for assessment by flow cytometry as described below at 18 hours. For analysis of metabolism, cells were analyzed using the Agilent Seahorse Assays as described below.

For Western blot analysis of phosphorylated and total expression levels of signaling molecules, activated cells (and non-activated controls) were washed twice with 1X HBSS and $3–5\times10^6$ cells were pelleted for lysis in mammalian protein extraction reagent (M-PER, Fisher). Protein concentration was normalized for loading based on a bicinchoninic acid (BCA) assay and mixed with NuPage LDS Sample Buffer (Life Technologies) before loading. Samples were run on a 4–12% Bis-Tris gradient gel (Life Technologies) using the Xcell Mini-cell electrophoresis system in 1X MES SDS Running Buffer (Life Technologies). Proteins were transferred to a nitrocellulose membrane using the Xcell II Blot Module and 1X Bolt Transfer Buffer with 20% methanol (Life Technologies). Blots were blocked with blocking buffer (LICOR) then incubated overnight with the indicated primary antibody, washed with TBS-T (Cell Signaling), and incubated for 1 hour with appropriate secondary antibodies in blocking buffer (LICOR). Blots were imaged using a LICOR Odyssey and quantified using ImageJ. For phosflow flow cytometry analysis of phosphorylated signaling molecules, naïve WT ($CD45.1^+$) and PSGL-$1^{-/-}$ ($CD90.1^+$) OT-I $CD8^+$ T cells were mixed 1:1 with each other and then with C57BL/6 splenocytes generated from uninfected female mice. T cells were activated in FACS tubes (BD Falcon) by the addition of 10 μM SIINFEKL peptide (GenScript) for the indicated time at 37°C. After activation, pre-warmed 1X BD Phosflow Fix Buffer I (BD) was immediately added to cells and incubated for 15 minutes at 37°C. Cells were washed with BD Phosflow Perm Wash and permeabilized by the addition of cold BD Phosflow Perm Buffer III while vortexing. After permeabilization, both surface markers and phosphorylated signaling molecules were stained simultaneously in BD Phosflow Perm Wash for 45 minutes. Cells were washed and fixed with 1% formaldehyde prior to data acquisition on a BD LSRFortessa X-20 (BD) and analyzed using FlowJo v10 software (BD).

T Cell activation (human): Cryopreserved healthy donor human PBMCs (purchased from iXcells Biotech) were thawed then rested for five hours at 37°C. After resting, cells were cultured in complete T cell media supplemented with 5 ng/mL each of recombinant human IL-7 and IL-15 (PeproTech) and 10 U/mL recombinant human IL-2 at a concentration of 1 × 10^6 $CD3^+$ cells/mL and stimulated with 6.25 μL/mL of ImmunoCult Human CD3/CD28 T cell activator (StemCell) for two days. On day 2, T cells were stained for assessment by flow cytometry as described and cytokine production was assessed following overnight restimulation with ImmunoCult in the presence of Brefeldin A and monensin.

Sts-1 western blot analysis: For Sts-1 Western blot analysis, cells were lysed in M-PER buffer (Thermo Scientific) containing protease/phosphatase inhibitor cocktail (Roche). Protein concentration was measured using a BCA assay (Pierce). Equivalent amounts of each sample were loaded on 4–12% Bis-Tris gels (Invitrogen), transferred to nitrocellulose membranes, and immunoblotted with antibodies against Sts-1 (Proteintech #19563–1-AP) and β-Actin (Cell Signaling #3700). IRDye®800-labeled goat anti-rabbit IgG and IRDye®680-labeled goat anti-mouse IgG (LI-COR) secondary antibodies were used and detected on an Odyssey CL_xsystem.

Flow Cytometry: In all stains, cells were pre-treated with 2.5 μg/mL anti-CD16/32 (Fc Block; 2.4G2; BioLegend, San Diego, CA) for 15 minutes before continuing with surface staining. For surface stains, 2×10^6 cells were stained for 20 min on ice. Cells were stained with the fluorochrome conjugated monoclonal antibodies as indicated (Table S1). Where indicated, cells were also stained with APC labeled-tetramers of H-2^b major histocompatibility complex class I loaded with $GP_{(33–41)}$, or BV421 labeled-tetramers of H-$2D^b$ major histocompatibility complex class I loaded with $NP_{(396–404)}$ provided by the NIH Tetramer Core Facility. After staining, cells were washed twice with 1X HBSS containing 3% FBS and 0.02% sodium azide and fixed with 1% formaldehyde. For staining of intracellular transcription factors, 2×10^6 cells were stained as above for surface markers. Following the surface stain, cells were permeabilized with eBioscience FoxP3 fixation buffer (ThermoFisher) overnight at 4°C, washed using eBioscience 1X Perm Wash (ThermoFisher), followed by intracellular staining for 45 minutes. Cells were then washed 2 times with 1X Perm Wash containing 0.02% sodium azide and fixed with 1% formaldehyde. Cells were stained with the fluorochrome conjugated monoclonal antibodies indicated in the table below. For staining of intracellular cytokines, 2×10^6 cells were stimulated with the indicated peptide (OVA: 5 μg/mL SIINFEKL peptide; $GP_{(33–41)}$: 2 μg/mL KAVYNFATM peptide; $NP_{(396–404)}$:2 μg/mL FQPQNGQFI; all from Genscript) or ImmunoCult (for human PBMCs, StemCell) overnight at 37°C, 5% CO_2 in the presence of GolgiPlug (BD Biosciences), Monensin (BioLegend), and 10 U/mL recombinant human IL-2. Cells were surface stained as above then fixed overnight at 4°C with FoxP3 fixation buffer (eBioscience), washed using Perm/Wash buffer (eBioscience) and stained for intracellular cytokines for 45 minutes at 4°C. Cells were stained with the fluorochrome conjugated monoclonal antibodies indicated in the table below. 1X Perm Wash containing 0.02% sodium azide and fixed with 1% formaldehyde. All data was acquired on a BD LSRFortessa X-20 (BD) and analyzed using FlowJo v10 software (BD). When protein expression ratios

were calculated, they were calculated using the relative median fluorescence intensity (MFI) of the indicated proteins.

Fluorescence microscopy and Amnis Imaging Flow Cytometry: CD3 and PSGL-1 localization studies: for Amnis imaging flow cytometry, naive OT-I $CD8^+$ T cells were enriched from WT or PSGL-$1^{-/-}$ splenocytes from 6–8 week old female mice using magnetic bead enrichment. For crosslinking, naïve OT-I cells or TK-1 cells were incubated with anti-CD3ε (145–2C11, BioXcell), anti-PSGL-1 (4RA10, BioXcell), or both for 15 minutes at 4°C. After washing, cells were crosslinked with biotinylated anti-hamster IgG (for anti-CD3; BD Pharmingen) and/or goat anti-rat IgG (for anti-PSGL-1, Sigma Aldrich) and incubated for 10 minutes at 37°C. After incubation, cells were fixed with 1% formaldehyde. CD3 localization was detected using FITC conjugated streptavidin (CALTAG Laboratories) and PSGL-1 localization was detected using anti-Rat IgG-PE (BioLegend) following a 30 minute incubation at 4°C. For fluorescence microscopy, stained TK-1 cells were plated on slides pre-coated with CellTak (Corning). For Amnis imaging flow cytometry, cells were imaged immediately using an Amnis Imaging Flow Cytometer.

PSGL-1, Zap70, and Sts-1 localization studies: naïve cells were incubated on plate-bound anti-CD3ε for 20 minutes at 37°C. After washing, cells were stained with anti-Sts-1 AF488 (19563–1-AP, Proteintech; in-house conjugated using APEX AF488 antibody labeling kits, ThermoFisher), anti-CD162 (4RA10, eBioscience), anti-CD3 BV421 (17A2, BioLegend), and anti-Zap70 (A15114B, BioLegend) before fixation in 1% formaldehyde.

For quantification by Amnis Imaging Flow Cytometry, samples were acquired using an ImageStreamX Mk11 (2 cameras) and INSPIRE v200.1.388.0 software. Images were assessed at a 40X objective in high resolution/low speed mode. 10,000 gated events ($Hoechst^+FITC^+$, in focus, single cells) were acquired per condition. For analysis, IDEAS v6.2.183.0 software was used and compensation and nuclear localization were calculated using the IDEAS wizard. The Amnis similarity score (a transformed Pearson's correlation coefficient[52]) was calculated from these data.

Seahorse: Assays were conducted in Seahorse XF RPMI Medium, pH 7.4 (Agilent) supplemented with sodium pyruvate [1 mM], L-glutamine [2 mM], and glucose [5 mM]. Seahorse XF plates were pre-coated with 22.4 ug/mL of Cell-Tak solution (Corning) as per manufacturer's instructions on the same day as the assay and 0.3×10^6 cells were seeded per well. For glycolytic rate assays: rotenone [0.0013 mM]/antimycin A [0.013 mM], and 2-DG [500 mM] prepared in supplemented Seahorse XF RPMI Medium were injected sequentially as indicated. Assays were conducted using an XFp (8 well) system and analyzed using WAVE software (Agilent).

Single-cell RNA-sequencing: Naïve WT ($CD45.1^+$) or PSGL-$1^{-/-}$ ($CD90.1^+$) OT-I $CD8^+$ T cells were activated with immobilized anti-CD3ε (145–2C11, BioXcell) and anti-CD28 (37.51, BioXcell)(5 μg/mL, each) for 3 days prior to transfer. 1×10^6 activated WT or PSGL-$1^{-/-}$ OT-I $CD8^+$ T cells were then injected I.V. into tumor-bearing C57BL/6 ($CD45.2^+/CD90.2^+$) mice, 7 days after inoculation with B16-OVA tumors. Six days after T cell transfer, live donor OT-I $CD8^+$ T cells were sorted by FACS from B16-OVA tumors.

Live sorted cells were immediately processed on a 10X Chromium (10X) to generate single cell 3' libraries using the 10X Single Cell 3' Reagent Kits v2 as per (manufacturer's instructions (Rev E, 2018). Data were acquired using a HiSeq 400 PE50 at the Institute for Genomic Medicine Facility at the University of California, San Diego.

scRNA-seq analysis: scRNA-seq data were aligned, counted, and aggregated using 10X Genomics Cell Ranger v2.2.0.[53] Both PSGL-$1^{-/-}$ OT-I and WT OT-I data sets were down-sampled to 2500 cells each, before integration was performed using canonical correlation analysis (CCA) with the *IntegrateData* function of Seurat v4.1.1.[54] The integrated data was scaled and visualized as Uniform Manifold Approximation and Projection for Dimension Reduction (UMAP) plots[55] with the *RunUMAP* function of Seurat using PCA as first-level dimension reduction method. A shared nearest neighbor (SNN) graph was then constructed by computing the Jaccard index between each cell and its 20 nearest neighbors based on the first 30 PCs, and clusters were identified by modularity maximization of the SNN graph using the *FindClusters* function of Seurat with a resolution of 0.5. SeqGeq (FlowJo, BD) was used in some analyses to assess expression changes within subgated "cell" populations. Data quality control was assessed using Seurat based on Satija Lab tutorials (https://satijalab.org/seurat/articles/integration_introduction.html). Each of the eight cell clusters identified were further divided into two sub-clusters corresponding to cells coming from PSGL-$1^{-/-}$ OT-I and WT OT-I, respectively, leading to a total of 16 sub-clusters. For each sub-cluster, differential expression analysis was performed to compare the expression levels of each gene in the cells in this sub-cluster (group A) with those of cells in the other 15 sub-clusters together (group B). We filtered out genes expressed in less than 25% of the cells in both groups and those with a two-sided Wilcoxon rank-sum test p-value > 0.01 with the *FindAllMarkers* function of Seurat. The top 10 most differentially expressed genes, in terms of log2 fold change, from each sub-cluster (as group A) were collected to produce a heatmap using the *DoHeatmap* function of Seurat. Expression levels of some genes in the two sub-clusters of each cell cluster were also compared with violin plots using the *VlnPlot* function of Seurat, with p-values computed using two-sided Wilcoxon rank-sum test and added to the violin plots using the *stat_compare_means* function of ggpubr v0.4.0.[56]

Proteomics and phosphoproteomics sample preparation: 5×10^6 naïve $CD8^+$ T cells were plated per well of a 6-well plate coated with 5 μg/mL anti-CD3ε antibody (145–2C11, BioXCell)(activated) or appropriate IgG control (naïve) and centrifuged for 1 minute at 300×g. Per biological replicate, cells were pooled from 2–3 individual mice. Cells were incubated for 15 minutes at 37°C, then placed directly on ice for removal by pipetting. Cell pellets were snap frozen at −80°C then lysed in 8M urea, 50 mM ammonium bicarbonate (ABC) and Benzonase. Cellular debris were removed and supernatant protein concentration was determined using a BCA protein assay (Thermo Scientific). Disulfide bridges were reduced with 5 mM tris(2-carboxyethyl)phosphine (TCEP) at 30°C for 60 min, and cysteines were subsequently alkylated with 15 mM iodoacetamide (IAA) in the dark at room temperature for 30 min. Urea was then diluted to 1 M urea using 50 mM ABC, and proteins were subjected to overnight digestion with mass spec grade Trypsin/Lys-C mix (Promega). Following digestion, samples were acidified with formic acid (FA) and subsequently peptides were desalted using AssayMap C18 cartridges mounted on an

AssayMap Bravo Platform (Agilent Technologies). Two biological replicates were pooled together to generate 100 micrograms of total peptide for TMT labeling and subsequent fractionation and phosphopeptide enrichment. Dried pooled sample was reconstituted in 20 mM ammonium formate pH ~10, and separated in 2 aliquots of 100 and 900 micrograms for total proteomics and phosphoproteomics fractionation. Total proteome TMT and phosphoproteome aliquots were fractionated using a Waters Acquity BEH C18 column (Total: 2.1× 15 cm, 1.7 μm pore size; Phospho: 4.6× 25 cm, 3.5 μm pore size) mounted on an M-Class Ultra Performance Liquid Chromatography (UPLC) system (Waters)(total) or Vanquish Horizon UPLC system (ThermoFisher). A total of 36 (total) or 12 fractions were collected and pooled in a non-contiguous manner into 18 total fractions and dried to completeness in a SpeedVac concentrator prior to mass spectrometry analysis. TMT-labeled phosphopeptides were enriched in an automated fashion using the AssayMAP Bravo Platform (Agilent Technologies).

LC-MS/MS analysis: Dried peptide fractions were reconstituted with 2% ACN, 0.1% FA and analyzed by LC-MS/MS using a Proxeon EASY nanoLC system (Thermo Fisher Scientific) coupled to an Orbitrap Fusion Lumos mass spectrometer (Thermo Fisher Scientific). Peptides were separated using an analytical C18 Aurora column (75μm × 250 mm, 1.6μm particles; IonOpticks) at a flow rate of 300 nL/min using a 75-min gradient: 1% to 6% B in 1 min, 6% to 23% B in 44 min, 23% to 34% B in 28 min, and 27% to 48% B in 2 min (A= FA 0.1%; B=80% ACN: 0.1% FA). The mass spectrometer was operated in positive data-dependent acquisition mode. MS1 spectra were measured in the Orbitrap with a resolution of 60,000, at accumulation gain control (AGC) target of 4e5 with maximum injection time of 50 ms, and within a mass range from 350 to 1500 m/z. Tandem MS was performed on the most abundant precursors with charge state between +2 and +7 by isolating them in the quadrupole with an isolation window of 0.7 m/z. Precursors were fragmented with higher-energy collisional dissociation (HCD) with normalized collision energy of 35% and the resulting fragments were detected in the Orbitrap at 50,000 resolution, at AGC of 1e5 and maximum injection time of 105 ms. The dynamic exclusion was set to 20 sec with a 10 ppm mass tolerance around the precursor. To increase confidence of the data, each fraction of total and enriched phosphopeptide were run in duplicates. All mass spectra were analyzed with MaxQuant software version 1.6.11.0. MS/MS spectra were searched against the Mus musculus Uniprot protein sequence database (downloaded in January 2020) and GPM cRAP sequences (commonly known protein contaminants). Reporter ion MS2 type was selected along with TMT 10plex option. Precursor mass tolerance was set to 20ppm and 4.5ppm for the first search where initial mass recalibration was completed and for the main search, respectively. Product ions were searched with a mass tolerance 0.5 Da. The maximum precursor ion charge state used for searching was 7. Carbamidomethylation of cysteine was searched as a fixed modification, while oxidation of methionine and acetylation of protein N-terminal were searched as variable modifications. Enzyme was set to trypsin in a specific mode and a maximum of two missed cleavages was allowed for searching. The target-decoy-based false discovery rate (FDR) filter for spectrum and protein identification was set to 1%. Statistical analysis of TMT total and phosphoproteome data were carried out using in-house R script (version 3.5.1, 64-bit), including R Bioconductor packages. First, TMT reporter

intensities were log2-transformed and normalized (loess normalization) across samples to account for systematic errors. Following normalization, all non-razor peptide sequences and precursor isolation interference (MaxQuant "PIF" column in evidence file) below 0.8 (total proteome) or 0.9 (phosphoproteome) were removed from the list. Phosphopeptide- and Protein-level quantification and statistical testing for differential abundance were performed using MSstatsTMT bioconductor package[57]. In MSstatsTMT experimental setting, the technical replicates were analyzed together as different 'mixtures'.

ATAC-sequencing: Naïve OT-I $CD8^+$ T cells were enriched from WT or PSGL-$1^{-/-}$ splenocytes from 6–8 week old female mice using magnetic bead enrichment. After enrichment, 1×10^6 naïve $CD8^+$ T cells were plated per well of a 24-well plate coated with 5 ug/mL anti-CD3 antibody (145–2C11, BioXCell) and centrifuged for 1 minute at 300×g. Cells were incubated for 2 hours at 37°C. ATAC-seq libraries were prepared following the omni-ATAC protocol[58] with minor changes. 50,000 cells were rinsed with 1XPBS and centrifuged at 400g for 3 minutes. Cells were resuspended in 50 µl lysis buffer (10 mM 1 M Tris-HCl pH 7.4, 10 mM NaCl, 3 mM $MgCl^2$, 0.1% NP40, 0.1% Tween 20, 0.01% Digitonin), and incubated at 4°C for 5 minutes, after which 1 mL rinsing buffer (10 mM Tris-HCl pH 7.4, 10 mM NaCl, 3 mM $MgCl^2$, 0.1% Tween 20) was added, then centrifuged at 1,000×g for 10 minutes at 4°C. After removing the supernatant, the nuclei were resuspended in 50 µL of transposition mix (25 µL of TD buffer [20 mM Tris-HCl pH 7.6, 10 mM MgCl2, 20% Dimethyl Formamide], 2.5 µL of 2 µM transposase 16.5 ml PBS, 0.5 µL 1% digitonin, 0.5 µL 10% Tween-20, 5 mL water) and incubated at 37 °C for 30 minutes. DNA was obtained with a Qiagen MinElute Kit (Qiagen). Libraries were prepared with KAPA HiFi High sensitivity Real-time PCR master mix. The ATAC library sequenced on an Illumina Novaseq 6000 sequencer (paired-end 50-bp reads) at the La Jolla Institute for Immunology sequencing core.

ATAC-seq analysis: ATAC-seq QC and analysis was performed by the Bioinformatics Core at Sanford Burnham Prebys Medical Discovery Institute. In brief, FASTQ files were generated following adaptor trimming (Cutadapt) and MultiQC was used to evaluate library quality. STAR was used to align ATAC-seq data to mouse genome B38, Ensembl v84 and Homer was used for peak calling and annotation. DESeq2 and Homer were used to identify differential peak analysis. IGV genome browser was used for peak visualization. Reproducible peaks were compared with public dataset[59] using BEDTools.[60]

QUANTIFICATION AND STATISTICAL ANALYSIS

Statistics—For *in vivo* studies, a power analysis was performed to determine the number of animals per group per experiment, assuming 80% power and two-sided 0.05 significance. For each experiment, the number of animals per group (n) are indicated in the figure legend. The number of replicate experiments is noted in each figure legend. Specific statistical analyses for big data sets are indicated in their specific methods section. For flow cytometry data, the normality of the population distribution was assessed using the Shapiro-Wilk normality test by GraphPad Prism 9 and determined the statistical approach used. Significant differences between normally distributed populations were assessed using a two-tailed, unpaired t-test. Significant differences between non-normally distributed populations were

assessed using a two-tailed Mann Whitney exact test. The tests performed are denoted in each figure legend and subsequent p-values are annotated in the associated figure. Error bars denote standard error of the mean (SEM).

Supplementary Material

Refer to Web version on PubMed Central for supplementary material.

ACKNOWLEDGMENTS

Thank you to the following individuals: Dr. Kristen Jepsen, Institute for Genomic Medicine; Dr. Kathleen Fisch, Center for Computational Biology & Bioinformatics at UC San Diego; Petrus de Jong; Bobby Ng; Yoav Altman; Amy Cortez; David Scott; Buddy Charbono; Andy Vasquez; and all Bradley lab members. This work was funded as follows. J.L.H.: American Cancer Society Postdoctoral Fellowship (PF-20–113-01-LIB) and T32 AI125209; E.-A.B.: The American Association of Immunologists Careers in Immunology Fellowship Program; L.M.B.: R01 AI106895, R21 CA249353, R21 CA216678, R03 CA252144, MRA 696326, DoD W81XWH-20–1-0324, and San Diego C3 2018 (with G.A.D.); and A.R.: AI040127 and AI109842. This work was supported in part by the NCI-Designated Cancer Center Support Grant, P30 CA030199, and the following Sanford Burnham Prebys Core facilities: Flow Cytometry, Vivarium, Histology, Bioinformatics, Proteomics, and Cancer Metabolism.

REFERENCES

1. McLane LM, Abdel-Hakeem MS, and Wherry EJ (2019). CD8 T cell exhaustion during chronic viral infection and cancer. Annu. Rev. Immunol. 37, 457–495. 10.1146/annurev-immunol-041015-055318. [PubMed: 30676822]
2. Baumeister SH, Freeman GJ, Dranoff G, and Sharpe AH (2016). Coinhibitory pathways in immunotherapy for cancer. Annu. Rev. Immunol. 34, 539–573. 10.1146/annurev-immunol-032414-112049. [PubMed: 26927206]
3. Zehn D, Thimme R, Lugli E, de Almeida GP, and Oxenius A (2022). Stem-like' precursors are the fount to sustain persistent CD8(+) T cell responses. Nat. Immunol. 23, 836–847. 10.1038/s41590-022-01219-w. [PubMed: 35624209]
4. Tinoco R, and Bradley LM (2017). Targeting the PSGL-1 pathway for immune modulation. Immunotherapy 9, 785–788. 10.2217/imt-2017-0078. [PubMed: 28877633]
5. Tinoco R, Otero DC, Takahashi AA, and Bradley LM (2017). PSGL-1: a new player in the immune checkpoint landscape. Trends Immunol. 38, 323–335. 10.1016/j.it.2017.02.002. [PubMed: 28262471]
6. Tinoco R, Carrette F, Barraza ML, Otero DC, Magaña J, Bosenberg MW, Swain SL, and Bradley LM (2016). PSGL-1 is an immune checkpoint regulator that promotes T cell exhaustion. Immunity 44, 1190–1203. 10.1016/j.immuni.2016.04.015. [PubMed: 27192578]
7. Tinoco R, Neubert EN, Stairiker CJ, Henriquez ML, and Bradley LM (2021). PSGL-1 is a T cell intrinsic inhibitor that regulates effector and memory differentiation and responses during viral infection. Front. Immunol. 12, 677824. 10.3389/fimmu.2021.677824. [PubMed: 34326837]
8. Cibrián D, and Sánchez-Madrid F (2017). CD69: from activation marker to metabolic gatekeeper. Eur. J. Immunol. 47, 946–953. 10.1002/eji.201646837. [PubMed: 28475283]
9. Shatrova AN, Mityushova EV, Vassilieva IO, Aksenov ND, Zenin VV, Nikolsky NN, and Marakhova II (2016). Time-dependent regulation of IL-2R alpha-chain (CD25) expression by TCR signal strength and IL-2-induced STAT5 signaling in activated human blood T lymphocytes. PLoS One 11, e0167215. 10.1371/journal.pone.0167215. [PubMed: 27936140]
10. Simon S, and Labarriere N (2017). PD-1 expression on tumor-specific T cells: friend or foe for immunotherapy? OncoImmunology 7, e1364828. 10.1080/2162402X.2017.1364828. [PubMed: 29296515]
11. Lee-Sayer SSM, Maeshima N, Dougan MN, Dahiya A, Arif AA, Dosanjh M, Maxwell CA, and Johnson P (2018). Hyaluronan-binding by CD44 reduces the memory potential of activated murine CD8 T cells. Eur. J. Immunol. 48, 803–814. 10.1002/eji.201747263. [PubMed: 29315518]

12. Zhao M, Kiernan CH, Stairiker CJ, Hope JL, Leon LG, van Meurs M, Brouwers-Haspels I, Boers R, Boers J, Gribnau J, et al. (2020). Rapid in vitro generation of bona fide exhausted CD8+ T cells is accompanied by Tcf7 promotor methylation. PLoS Pathog. 16, e1008555. 10.1371/journal.ppat.1008555. [PubMed: 32579593]
13. Zehn D, Lee SY, and Bevan MJ (2009). Complete but curtailed T-cell response to very low-affinity antigen. Nature 458, 211–214. 10.1038/nature07657. [PubMed: 19182777]
14. Motamedi M, Xu L, and Elahi S (2016). Correlation of transferrin receptor (CD71) with Ki67 expression on stimulated human and mouse T cells: the kinetics of expression of T cell activation markers. J. Immunol. Methods 437, 43–52. 10.1016/j.jim.2016.08.002. [PubMed: 27555239]
15. Sánchez-Madrid F, and del Pozo MA (1999). Leukocyte polarization in cell migration and immune interactions. EMBO J. 18, 501–511. 10.1093/emboj/18.3.501. [PubMed: 9927410]
16. Carpino N, Turner S, Mekala D, Takahashi Y, Zang H, Geiger TL, Doherty P, and Ihle JN (2004). Regulation of ZAP-70 activation and TCR signaling by two related proteins, Sts-1 and Sts-2. Immunity 20, 37–46. 10.1016/s1074-7613(03)00351-0. [PubMed: 14738763]
17. Zhou W, Yin Y, Weinheimer AS, Kaur N, Carpino N, and French JB (2017). Structural and functional characterization of the histidine phosphatase domains of human sts-1 and sts-2. Biochemistry (Moscow, Russ. Fed.) 56, 4637–4645. 10.1021/acs.biochem.7b00638.
18. Menk AV, Scharping NE, Moreci RS, Zeng X, Guy C, Salvatore S, Bae H, Xie J, Young HA, Wendell SG, and Delgoffe GM (2018). Early TCR signaling induces rapid aerobic glycolysis enabling distinct acute T cell effector functions. Cell Rep. 22, 1509–1521. 10.1016/j.celrep.2018.01.040. [PubMed: 29425506]
19. Chen Z, Ji Z, Ngiow SF, Manne S, Cai Z, Huang AC, Johnson J, Staupe RP, Bengsch B, Xu C, et al. (2019). TCF-1-Centered transcriptional network drives an effector versus exhausted CD8 T cell-fate decision. Immunity 51, 840–855.e5. 10.1016/j.immuni.2019.09.013. [PubMed: 31606264]
20. Hudson WH, Gensheimer J, Hashimoto M, Wieland A, Valanparambil RM, Li P, Lin JX, Konieczny BT, Im SJ, Freeman GJ, et al. (2019). Proliferating transitory T cells with an effector-like transcriptional signature emerge from PD-1(+) stem-like CD8(+) T cells during chronic infection. Immunity 51, 1043–1058.e4. 10.1016/j.immuni.2019.11.002. [PubMed: 31810882]
21. Wang Y, Hu J, Li Y, Xiao M, Wang H, Tian Q, Li Z, Tang J, Hu L, Tan Y, et al. (2019). The transcription factor TCF1 preserves the effector function of exhausted CD8 T cells during chronic viral infection. Front. Immunol. 10, 169. 10.3389/fimmu.2019.00169. [PubMed: 30814995]
22. Sade-Feldman M, Yizhak K, Bjorgaard SL, Ray JP, de Boer CG, Jenkins RW, Lieb DJ, Chen JH, Frederick DT, Barzily-Rokni M, et al. (2018). Defining T cell states associated with response to checkpoint immunotherapy in melanoma. Cell 175, 998–1013.e20. 10.1016/j.cell.2018.10.038. [PubMed: 30388456]
23. Alfei F, Kanev K, Hofmann M, Wu M, Ghoneim HE, Roelli P, Utzschneider DT, von Hoesslin M, Cullen JG, Fan Y, et al. (2019). TOX reinforces the phenotype and longevity of exhausted T cells in chronic viral infection. Nature 571, 265–269. 10.1038/s41586-019-1326-9. [PubMed: 31207605]
24. Scott AC, Dündar F, Zumbo P, Chandran SS, Klebanoff CA, Shakiba M, Trivedi P, Menocal L, Appleby H, Camara S, et al. (2019). TOX is a critical regulator of tumour-specific T cell differentiation. Nature 571, 270–274. 10.1038/s41586-019-1324-y. [PubMed: 31207604]
25. Seo H, Chen J, González-Avalos E, Samaniego-Castruita D, Das A, Wang YH, López-Moyado IF, Georges RO, Zhang W, Onodera A, et al. (2019). TOX and TOX2 transcription factors cooperate with NR4A transcription factors to impose CD8(+) T cell exhaustion. Proc. Natl. Acad. Sci. USA 116, 12410–12415. 10.1073/pnas.1905675116. [PubMed: 31152140]
26. Yao C, Sun HW, Lacey NE, Ji Y, Moseman EA, Shih HY, Heuston EF, Kirby M, Anderson S, Cheng J, et al. (2019). Single-cell RNA-seq reveals TOX as a key regulator of CD8(+) T cell persistence in chronic infection. Nat. Immunol. 20, 890–901. 10.1038/s41590-019-0403-4. [PubMed: 31209400]
27. Obar JJ, Jellison ER, Sheridan BS, Blair DA, Pham QM, Zickovich JM, and Lefrançois L (2011). Pathogen-induced inflammatory environment controls effector and memory CD8+ T cell differentiation. J. Immunol. 187, 4967–4978. 10.4049/jimmunol.1102335. [PubMed: 21987662]

28. Khan O, Giles JR, McDonald S, Manne S, Ngiow SF, Patel KP, Werner MT, Huang AC, Alexander KA, Wu JE, et al. (2019). TOX transcriptionally and epigenetically programs CD8(+) T cell exhaustion. Nature 571, 211–218. 10.1038/s41586-019-1325-x. [PubMed: 31207603]
29. Wherry EJ, Blattman JN, Murali-Krishna K, van der Most R, and Ahmed R (2003). Viral persistence alters CD8 T-cell immunodominance and tissue distribution and results in distinct stages of functional impairment. J. Virol. 77, 4911–4927. 10.1128/jvi.77.8.4911-4927.2003. [PubMed: 12663797]
30. Raué HP, and Slifka MK (2009). CD8+ T cell immunodominance shifts during the early stages of acute LCMV infection independently from functional avidity maturation. Virology 390, 197–204. 10.1016/j.virol.2009.05.021. [PubMed: 19539966]
31. Miller BC, Sen DR, Al Abosy R, Bi K, Virkud YV, LaFleur MW, Yates KB, Lako A, Felt K, Naik GS, et al. (2019). Subsets of exhausted CD8(+) T cells differentially mediate tumor control and respond to checkpoint blockade. Nat. Immunol. 20, 326–336. 10.1038/s41590-019-0312-6. [PubMed: 30778252]
32. Utzschneider DT, Gabriel SS, Chisanga D, Gloury R, Gubser PM, Vasanthakumar A, Shi W, and Kallies A (2020). Early precursor T cells establish and propagate T cell exhaustion in chronic infection. Nat. Immunol. 21, 1256–1266. 10.1038/s41590-020-0760-z. [PubMed: 32839610]
33. Lee H, Jeong S, and Shin EC (2022). Significance of bystander T cell activation in microbial infection. Nat. Immunol. 23, 13–22. 10.1038/s41590-021-00985-3. [PubMed: 34354279]
34. Nevala WK, Vachon CM, Leontovich AA, Scott CG, Thompson MA, and Markovic SN; Melanoma Study Group of the Mayo Clinic Cancer Center (2009). evidence of systemic Th2-driven chronic inflammation in patients with metastatic melanoma. Clin. Cancer Res. 15, 1931–1939. 10.1158/1078-0432.CCR-08-1980. [PubMed: 19240164]
35. McLane LM, Ngiow SF, Chen Z, Attanasio J, Manne S, Ruthel G, Wu JE, Staupe RP, Xu W, Amaravadi RK, et al. (2021). Role of nuclear localization in the regulation and function of T-bet and Eomes in exhausted CD8 T cells. Cell Rep. 35, 109120. 10.1016/j.celrep.2021.109120. [PubMed: 33979613]
36. Buggert M, Tauriainen J, Yamamoto T, Frederiksen J, Ivarsson MA, Michaëlsson J, Lund O, Hejdeman B, Jansson M, Sönnerborg A, et al. (2014). T-bet and Eomes are differentially linked to the exhausted phenotype of CD8+ T cells in HIV infection. PLoS Pathog. 10, e1004251. 10.1371/journal.ppat.1004251. [PubMed: 25032686]
37. Li J, He Y, Hao J, Ni L, and Dong C (2018). High levels of Eomes promote exhaustion of anti-tumor CD8(+) T cells. Front. Immunol. 9, 2981. 10.3389/fimmu.2018.02981. [PubMed: 30619337]
38. Sekine T, Perez-Potti A, Nguyen S, Gorin JB, Wu VH, Gostick E, Llewellyn-Lacey S, Hammer Q, Falck-Jones S, Vangeti S, et al. (2020). TOX is expressed by exhausted and polyfunctional human effector memory CD8(+) T cells. Sci. Immunol. 5, eaba7918. 10.1126/sciimmunol.aba7918. [PubMed: 32620560]
39. Dammeijer F, van Gulijk M, Mulder EE, Lukkes M, Klaase L, van den Bosch T, van Nimwegen M, Lau SP, Latupeirissa K, Schetters S, et al. (2020). The PD-1/PD-L1-checkpoint restrains T cell immunity in tumor-draining lymph nodes. Cancer Cell 38, 685–700.e8. 10.1016/j.ccell.2020.09.001. [PubMed: 33007259]
40. Kamphorst AO, Wieland A, Nasti T, Yang S, Zhang R, Barber DL, Konieczny BT, Daugherty CZ, Koenig L, Yu K, et al. (2017). Rescue of exhausted CD8 T cells by PD-1-targeted therapies is CD28-dependent. Science 355, 1423–1427. 10.1126/science.aaf0683. [PubMed: 28280249]
41. Odorizzi PM, Pauken KE, Paley MA, Sharpe A, and Wherry EJ (2015). Genetic absence of PD-1 promotes accumulation of terminally differentiated exhausted CD8+ T cells. J. Exp. Med. 212, 1125–1137. 10.1084/jem.20142237. [PubMed: 26034050]
42. Keir ME, Freeman GJ, and Sharpe AH (2007). PD-1 regulates self-reactive CD8+ T cell responses to antigen in lymph nodes and tissues. J. Immunol. 179, 5064–5070. 10.4049/jimmunol.179.8.5064. [PubMed: 17911591]
43. Latchman YE, Liang SC, Wu Y, Chernova T, Sobel RA, Klemm M, Kuchroo VK, Freeman GJ, and Sharpe AH (2004). PD-L1-deficient mice show that PD-L1 on T cells, antigen-presenting cells, and host tissues negatively regulates T cells. Proc. Natl. Acad. Sci. USA 101, 10691–10696. 10.1073/pnas.0307252101. [PubMed: 15249675]

44. Okazaki T, and Honjo T (2007). PD-1 and PD-1 ligands: from discovery to clinical application. Int. Immunol. 19, 813–824. 10.1093/intimm/dxm057. [PubMed: 17606980]
45. Johnston RJ, Su LJ, Pinckney J, Critton D, Boyer E, Krishnakumar A, Corbett M, Rankin AL, Dibella R, Campbell L, et al. (2019). VISTA is an acidic pH-selective ligand for PSGL-1. Nature 574, 565–570. 10.1038/s41586-019-1674-5. [PubMed: 31645726]
46. Fransen MF, Schoonderwoerd M, Knopf P, Camps MG, Hawinkels LJ, Kneilling M, van Hall T, and Ossendorp F (2018). Tumor-draining lymph nodes are pivotal in PD-1/PD-L1 checkpoint therapy. JCI Insight 3, e124507. 10.1172/jci.insight.124507. [PubMed: 30518694]
47. Veerman KM, Williams MJ, Uchimura K, Singer MS, Merzaban JS, Naus S, Carlow DA, Owen P, Rivera-Nieves J, Rosen SD, and Ziltener HJ (2007). Interaction of the selectin ligand PSGL-1 with chemokines CCL21 and CCL19 facilitates efficient homing of T cells to secondary lymphoid organs. Nat. Immunol. 8, 532–539. [PubMed: 17401367]
48. Wang L, Rubinstein R, Lines JL, Wasiuk A, Ahonen C, Guo Y, Lu LF, Gondek D, Wang Y, Fava RA, et al. (2011). VISTA, a novel mouse Ig superfamily ligand that negatively regulates T cell responses. J. Exp. Med. 208, 577–592. 10.1084/jem.20100619. [PubMed: 21383057]
49. ElTanbouly MA, Zhao Y, Nowak E, Li J, Schaafsma E, Le Mercier I, Ceeraz S, Lines JL, Peng C, Carriere C, et al. (2020). VISTA is a checkpoint regulator for naive T cell quiescence and peripheral tolerance. Science 367, eaay0524. 10.1126/science.aay0524. [PubMed: 31949051]
50. Flies DB, Han X, Higuchi T, Zheng L, Sun J, Ye JJ, and Chen L (2014). Coinhibitory receptor PD-1H preferentially suppresses CD4(+) T cell-mediated immunity. J. Clin. Invest. 124, 1966–1975. 10.1172/JCI74589. [PubMed: 24743150]
51. Yuan L, Tatineni J, Mahoney KM, and Freeman GJ (2021). VISTA: a mediator of quiescence and a promising target in cancer immunotherapy. Trends Immunol. 42, 209–227. 10.1016/j.it.2020.12.008. [PubMed: 33495077]
52. George TC, Fanning SL, Fitzgerald-Bocarsly P, Medeiros RB, High-fill S, Shimizu Y, Hall BE, Frost K, Basiji D, Ortyn WE, et al. (2006). Quantitative measurement of nuclear translocation events using similarity analysis of multispectral cellular images obtained in flow. J. Immunol. Methods 311, 117–129. 10.1016/j.jim.2006.01.018. [PubMed: 16563425]
53. Srivatsan SR, McFaline-Figueroa JL, Ramani V, Saunders L, Cao J, Packer J, Pliner HA, Jackson DL, Daza RM, Christiansen L, et al. (2020). Massively multiplex chemical transcriptomics at single-cell resolution. Science 367, 45–51. 10.1126/science.aax6234. [PubMed: 31806696]
54. Hao Y, Hao S, Andersen-Nissen E, Mauck WM 3rd, Zheng S, Butler A, Lee MJ, Wilk AJ, Darby C, Zager M, et al. (2021). Integrated analysis of multimodal single-cell data. Cell 184, 3573–3587.e29. 10.1016/j.cell.2021.04.048. [PubMed: 34062119]
55. Leland McInnes JH, and James M (2020). UMAP: Uniform Manifold approximation and projection for dimension reduction. Preprint at arXiv. 10.48550/arXiv.1802.03426.
56. Kassambara A (2020). Ggpubr: 'ggplot2' Based Publication Ready Plots. https://CRAN.R-project.org/package=ggpubr.
57. Huang T, Choi M, Tzouros M, Golling S, Pandya NJ, Banfai B, Dunkley T, and Vitek O (2020). MSstatsTMT: statistical detection of differentially abundant proteins in experiments with isobaric labeling and multiple mixtures. Mol. Cell. Proteomics 19, 1706–1723. 10.1074/mcp.RA120.002105. [PubMed: 32680918]
58. Corces MR, Trevino AE, Hamilton EG, Greenside PG, Sinnott-Armstrong NA, Vesuna S, Satpathy AT, Rubin AJ, Montine KS, Wu B, et al. (2017). An improved ATAC-seq protocol reduces background and enables interrogation of frozen tissues. Nat. Methods 14, 959–962. 10.1038/nmeth.4396. [PubMed: 28846090]
59. Yu B, Zhang K, Milner JJ, Toma C, Chen R, Scott-Browne JP, Pereira RM, Crotty S, Chang JT, Pipkin ME, et al. (2017). Epigenetic landscapes reveal transcription factors that regulate CD8(+) T cell differentiation. Nat. Immunol. 18, 573–582. 10.1038/ni.3706. [PubMed: 28288100]
60. Quinlan AR, and Hall IM (2010). BEDTools: a flexible suite of utilities for comparing genomic features. Bioinformatics 26, 841–842. 10.1093/bioinformatics/btq033. [PubMed: 20110278]

Highlights

- PSGL-1 restrains TCR signaling and glycolytic potential of $CD8^+$ T cells
- PSGL-1 deficiency limits $CD8^+$ T cell exhaustion and supports precursor populations
- Co-ligation of PSGL-1 and the TCR promotes T cell exhaustion in $CD8^+$ T cells
- PSGL-1 therapeutic blockade promotes T cell responses and melanoma tumor control

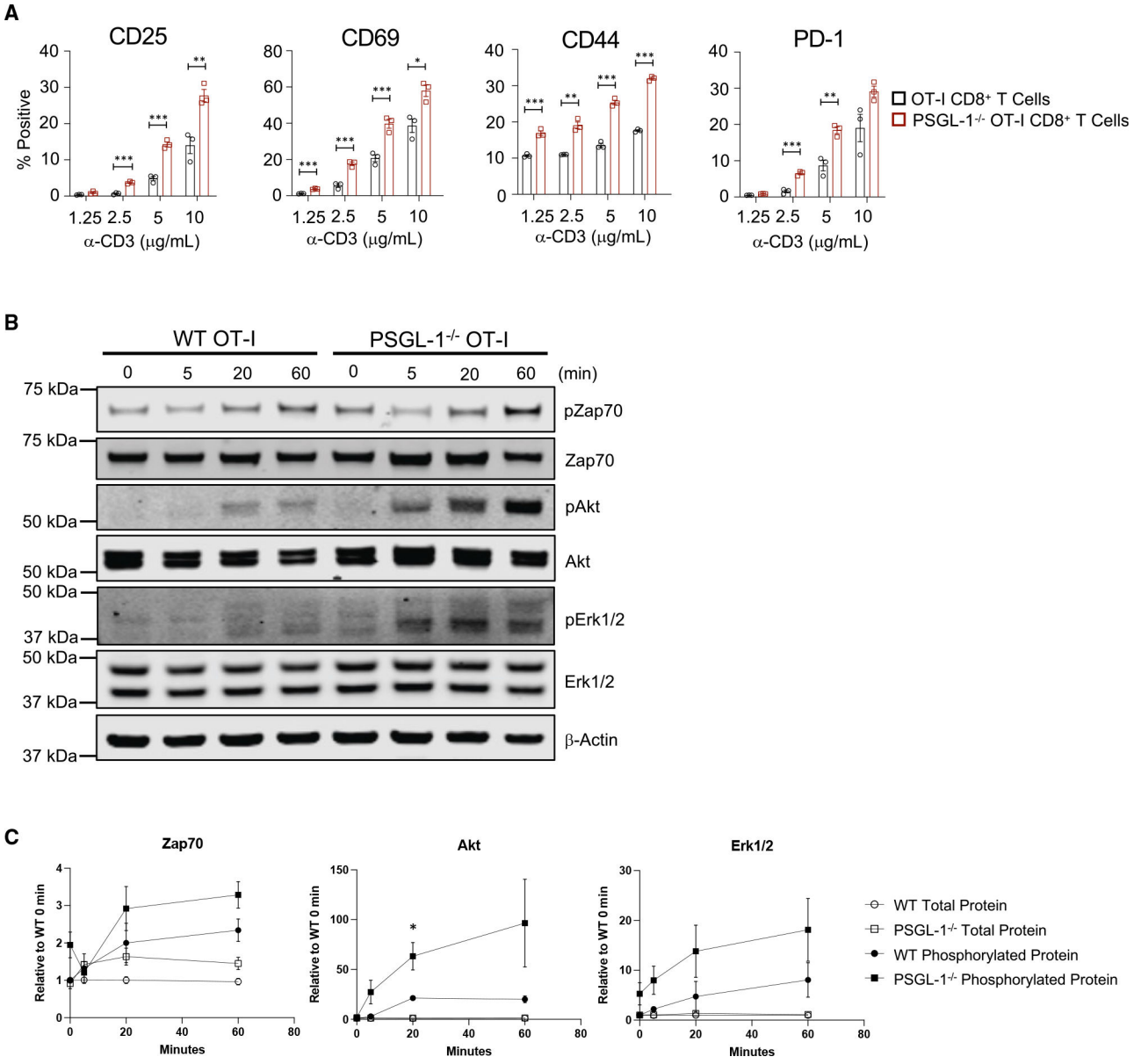

Figure 1. PSGL-1 restrains TCR signaling

(A) Frequencies of OT-I WT and PSGL-1$^{-/-}$ CD8^{+} T cells expressing activation markers at 18 h stimulation with anti-CD3ε antibody. Each dot represents an individual mouse. Experiments were performed 2×.

(B) Western blot of phosphorylated and total levels of Zap70, Erk1/2, AKT, and GAPDH in WT and PSGL-1$^{-/-}$ OT-I cells stimulated for the indicated time with anti-CD3ε antibody.

(C) Relative levels of phosphorylated Zap70, Erk1/2, and AKT, normalized to β-actin and relative to the specific protein of interest value in WT samples at 0 min for each blot. Experiments were performed 3×, 3 mice pooled/genotype, per experiment. (A–C) All data are parametric data except pAkt at 5 min. For parametric data, unpaired t tests were performed; Mann-Whitney test used for non-parametric data. Error bars are SEM. *p < 0.05, **p < 0.01, ***p < 0.005.

See also Figure S1.

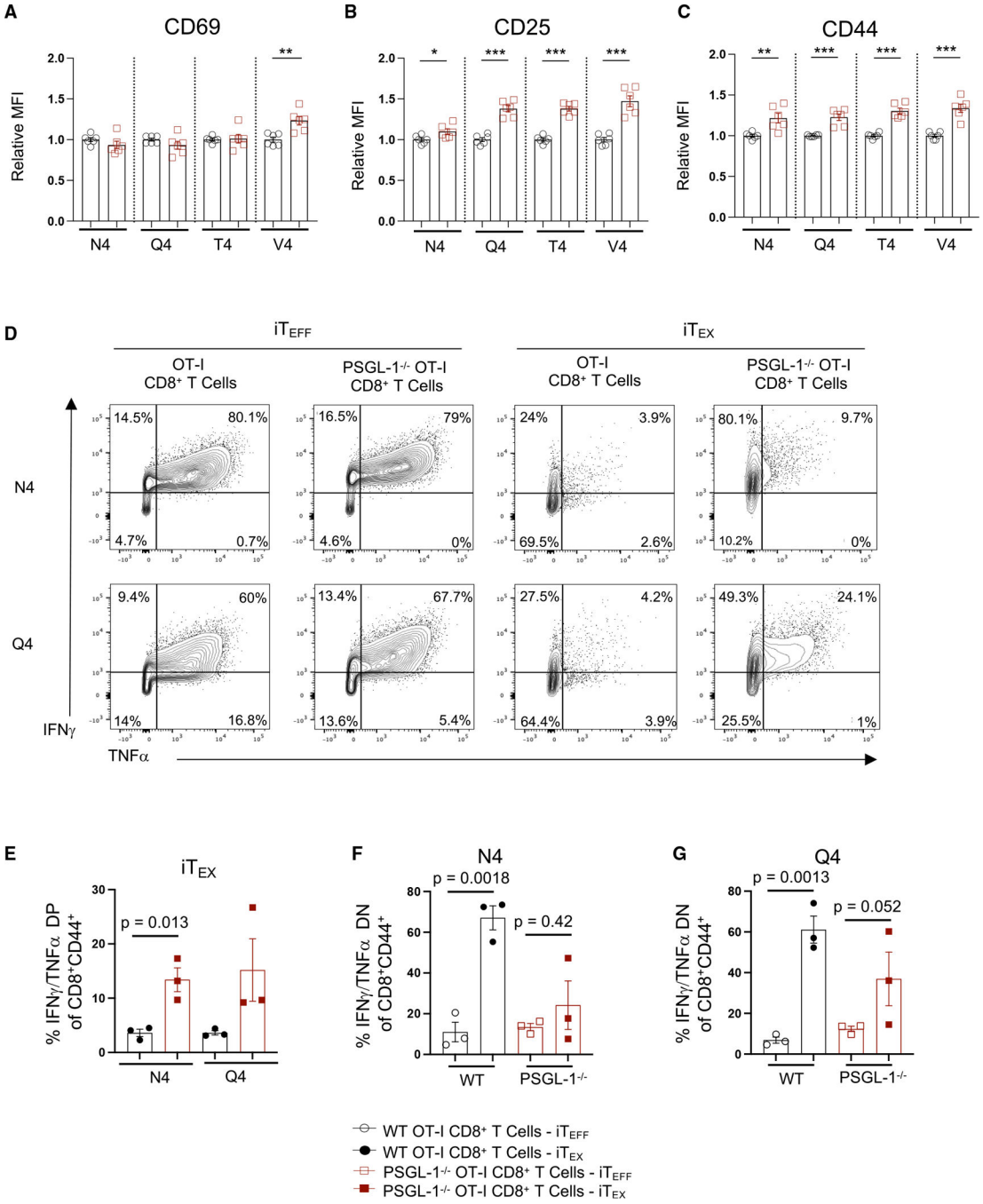

Figure 2. PSGL-1 deficiency promotes increased TCR signaling sensitivity

WT and PSGL-1$^{-/-}$ OT-I CD8^{+} T cells were stimulated with ovalbumin (OVA) peptide-pulsed activated splenocytes.

(A–C) Expression of (A) CD69, (B) CD25, and (C) CD44 was assessed by flow cytometry. OVA peptides of varying TCR affinities were used for stimulation: N4 (SIINFEKL), Q4 (SIIQFEKL), T4 (SIITFEKL), or V4 (SIIVFEKL).

(D–F) WT and PSGL-$1^{-/-}$ OT-I cells were cultured under effector (single stimulation; iT_{EFF}) or exhaustion conditions (repeated stimulation; iT_{EX}) with N4, Q4, T4, or V4 OVA peptides.

(D) Flow cytometry plots of IFNγ and TNF-α production by cultured WT and PSGL-$1^{-/-}$ OT-I cells restimulated on day 5 with SIINFEKL for 5 h.

(E) Frequency of double-positive IFNγ- and TNF-α-producing OT-I cells from WT (black circles) or PSGL-$1^{-/-}$ mice (red squares) following iT_{EX} culture with either SIINFEKL or SIIQFEKL peptide.

(F) Frequency of double-negative (non-IFNγ- or -TNF-α-producing) OT-I cells from WT or PSGL-$1^{-/-}$ mice following iT_{EFF} (open symbols) or iT_{EX} (closed symbols) culture with N4 peptide.

(G) Frequency of double-negative (non-IFNγ- or TNFα-producing) OT-I cells from WT or PSGL-$1^{-/-}$ mice following iT_{EFF} (open symbols) or iT_{EX} (closed symbols) culture with Q4 peptide.

(A–F) Each dot represents an individual experiment from a pooling of 1–2 mice/genotype/experiment, experiments were performed 3×. Data are parametric; unpaired t tests were performed. Error bars are SEM. *$p < 0.05$, **$p < 0.01$, ***$p < 0.005$.

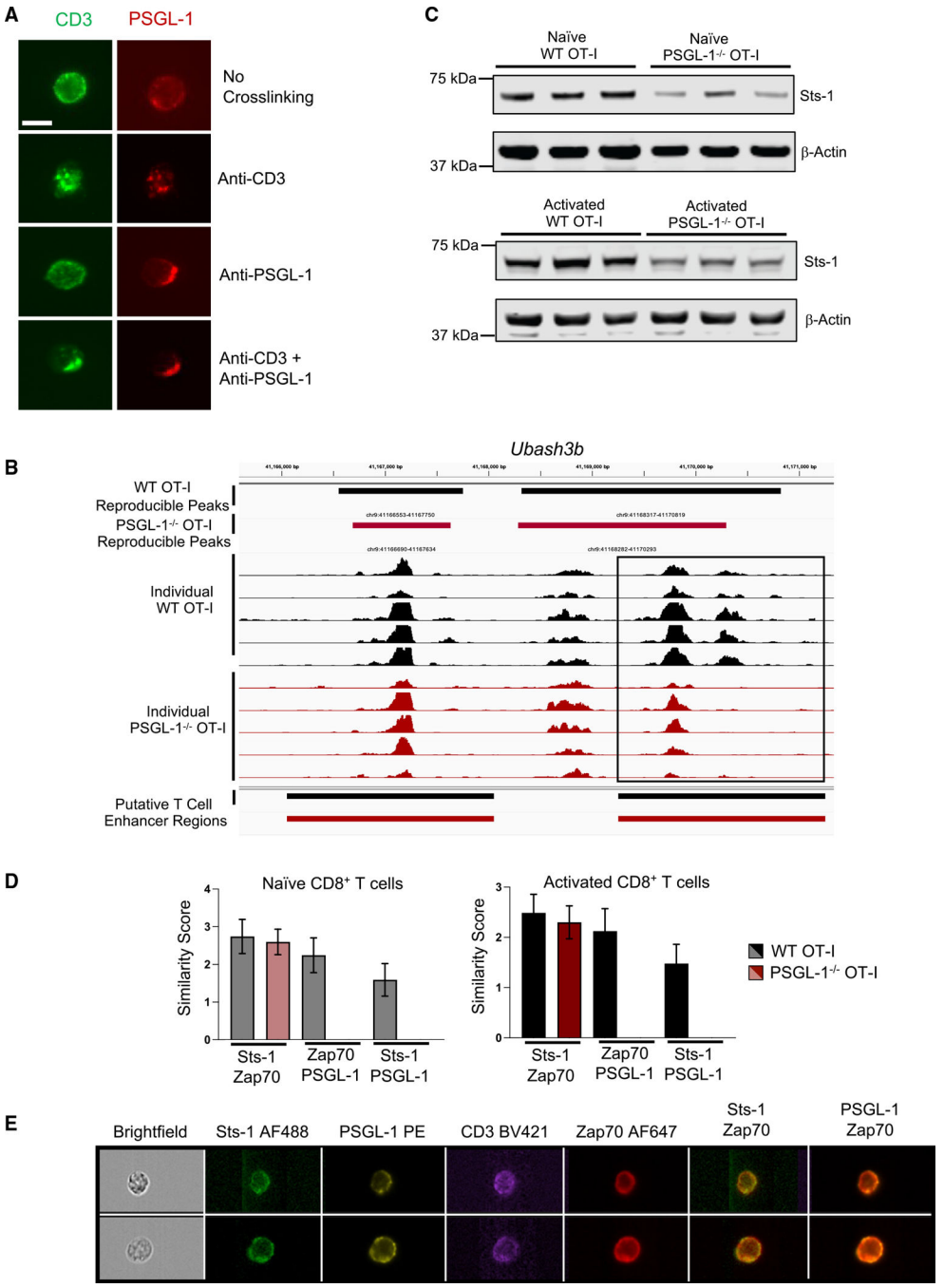

Figure 3. PSGL-1 co-localizes with the TCR, Zap70, and the Zap70 inhibitor Sts-1

(A) Immunofluorescence staining (40× magnification, scale bar of 10 μm) of CD3 (green) and PSGL-1 (red) on $CD8^+$ TK-1 cells before or after crosslinking with CD3 and/or PSGL-1 antibodies. Experiments were performed 2×.

(B) Chromatin accessibility within the *Ubash3b* gene region in WT OT-I cells (black) or PSGL-$1^{-/-}$ OT-I cells (red). Biological replicates prepared from 2 separate experiments.

(C) Western blot of Sts-1 and β-actin expression in naive (top) or 2 day activated (bottom) WT and PSGL-1$^{-/-}$ OT-I CD8^{+} T cells. Each band is a biologic replicate. Experiments were performed 2×.

(D and E) Imaging flow cytometry analysis of Sts-1, PSGL-1, CD3, and Zap70 localization and co-localization in 10,000 naive and activated WT and PSGL-1$^{-/-}$ OT-I CD8^{+} T cells.

(D) Similarity scores of Sts-1, Zap70, and PSGL-1 expression in naive (left) or 20 min activated (right) WT (gray/black) and PSGL-1$^{-/-}$ (light red, red) OT-I cells. Error bars are median absolute deviation (MAD).

(E) Representative images from (D) in two WT OT-I CD8^{+} T cells.

Experiment performed 2×. See also Figures S3 and S4.

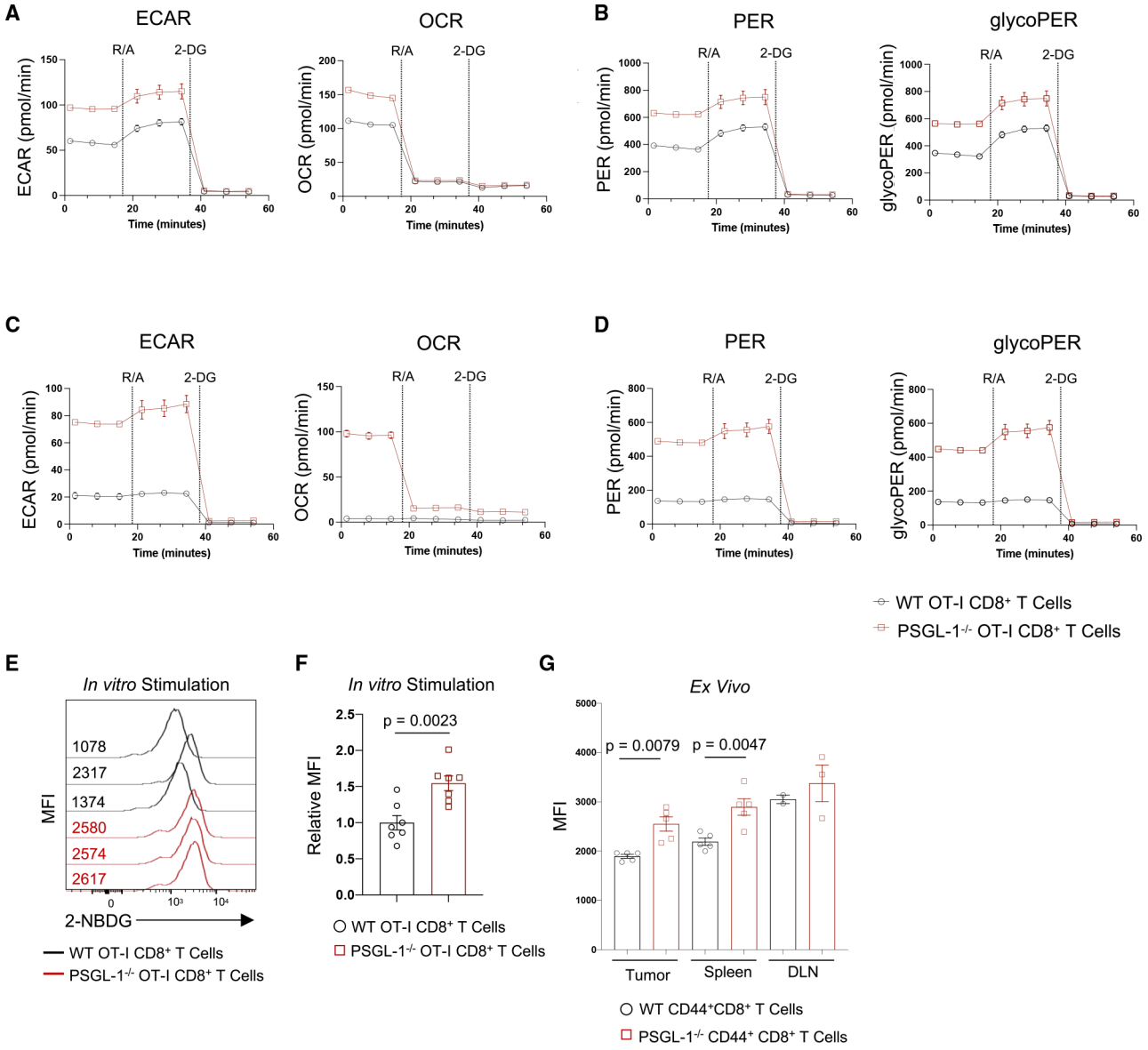

Figure 4. PSGL-1 restrains glycolysis in CD8$^+$ T cells

(A) Extracellular acidification rate (ECAR) and oxygen consumption rate (OCR) were assessed using the Seahorse Glycolytic Rate Assay in 3 day activated WT or PSGL-1$^{-/-}$ OT-I CD8$^+$ T cells.

(B) Proton efflux rates (PERs) and glycolytic PER (glycoPER) calculated based on (A).

(C) ECAR and OCR were assessed for iT$_{EX}$ OT-I cells or PSGL-1$^{-/-}$ OT-I cells on day 5.

(D) PER and glycoPER calculated based on (C).

(A)–(D) are representative of >3 experiments.

(E and F) Histograms (E) and graph (F) of 2-NBDG uptake in OT-I or PSGL-1$^{-/-}$ OT-I cells after 2 h stimulation with SIINFEKL peptide; each line/dot represents an individual mouse. Data are normally distributed.

(G) Graph of *ex vivo* 2-NBDG MFI values in CD44$^+$CD8$^+$ T cells from tumors, spleens, or tumor draining lymph nodes (DLNs) of WT or PSGL-1$^{-/-}$ mice bearing YUMM1.5 tumors.

Data in (D) and (G) are parametric except for WT tumors and DLN. For parametric data, unpaired t tests were performed; Mann-Whitney test used for non-parametric data. Error bars are SEM. Each dot in tumors and spleens represents an individual mouse; DLN represents a pool. Experiments were performed 2×.

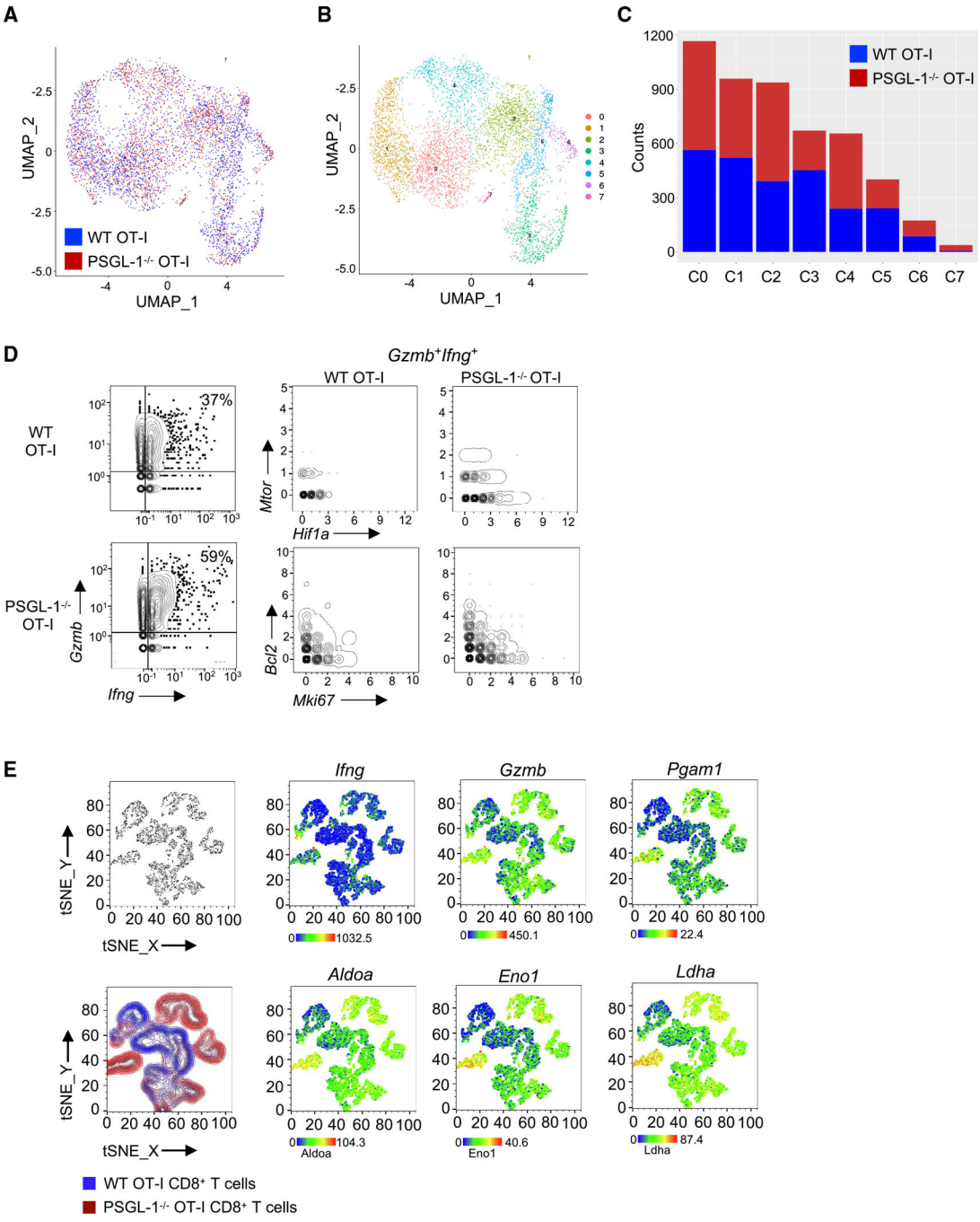

Figure 5. Single-cell sequencing reveals enhanced metabolic state of intratumoral PSGL-1$^{-/-}$ CD8^{+} T cells

1×10^6 activated WT OT-I (CD45.1^{+}) or PSGL-1$^{-/-}$ OT-I (CD90.1^{+}) T cells were injected into C57BL/6 mice 7 days after B16-OVA injection, and donor OT-I cells were sorted from tumors 6 days later for single-cell RNA sequencing.

(A) UMAP analysis (Seurat) of TILs.

(B and C) Composition analysis showing the breakdown of WT OT-I cells (pink) vs. PSGL-1$^{-/-}$ OT-I cells (green) overlaying the UMAP (B) and the number of counts of each per cluster (C).

(D) SeqGeq analysis of *Gzmb* and *Ifng* expression in WT and PSGL-1$^{-/-}$ OT-I cells (left). Top right: gene expression of *Mtor* and *Hif1a* in *Gzmb*$^{+}$*Ifng*$^{+}$ WT and PSGL-1$^{-/-}$ OT-I cells. Bottom right: gene expression of *Bcl2* and *Mki67* in *Gzmb*$^{+}$*Ifng*$^{+}$ WT and PSGL-1$^{-/-}$ OT-I CD8^{+} T cells.

(E) SeqGeq tSNE clustering of WT (blue) and PSGL-1$^{-/-}$ (red) OT-I cell libraries. Gene expression overlays of *Ifng*, *Gzmb*, *Pgam1*, *Aldoa*, *Eno1*, and *Ldha* in 1,000 single cells per condition from 6 mice per genotype.

See also Figure S5.

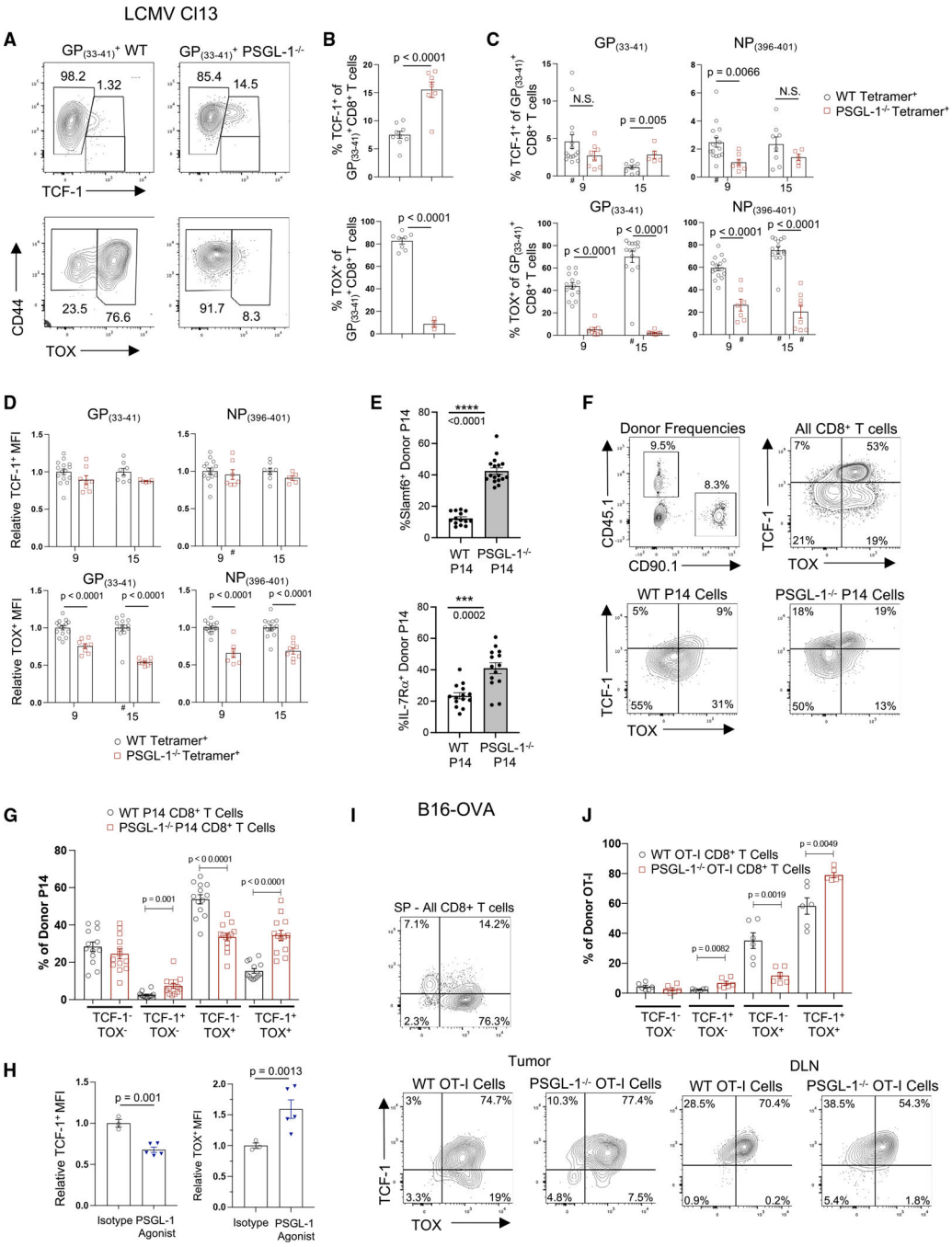

Figure 6. PSGL-1 limits TCF-1 and promotes TOX expression in CD8$^+$ T cells during chronic virus infection and cancer

(A) TCF-1 or TOX vs. CD44 expression in GP$_{(33–41)}$-specific CD8$^+$ T cells from spleens of WT or PSGL-1$^{-/-}$ mice 15 dpi with LCMV Cl13.

(B) Frequencies of TCF-1$^+$ (top) or TOX$^+$ (bottom) GP$_{(33–41)}{}^+$ CD8$^+$ T cells in spleens of WT or PSGL-1$^{-/-}$ mice 15 dpi.

(C) Frequencies of TCF-1$^+$ (top) or TOX$^+$ (bottom) GP$_{(33–41)}{}^+$ or NP$_{(396–404)}{}^+$ CD8$^+$ T cells in blood of WT or *PSGL-1*$^{-/-}$ mice on 9 and 15 dpi.

(D) The relative per-cell expression (MFI) of TCF-1^{+} (top) or TOX^{+} (bottom) GP$_{(33–41)}{}^{+}$ or NP$_{(396–404)}{}^{+}$ CD8^{+} T cells in blood of WT or PSGL-1$^{-/-}$ mice on 9 and 15 dpi.
(E) WT mice received a 1:1 mix of WT and PSGL-1$^{-/-}$ CD8^{+} P14 cells and infected with LCMV Cl13. Slamf6 and IL-7Rα expression on donor T cells in blood was assessed 60 dpi.
(F) Frequency of donor WT P14 and PSGL-1$^{-/-}$ P14 T cells within CD8^{+} T cells in blood on 60 dpi (top left). TCF-1 and TOX staining in CD8^{+} T cells (top right), WT P14 cells (bottom left), and PSGL-1$^{-/-}$ P14 cells (bottom right).
(G) Frequency of donor P14 cells expressing combinations of TCF-1 and TOX.
(H) Relative per-cell expression (MFI) of TCF-1^{+} (top) or TOX^{+} (bottom) GP$_{(33–41)}{}^{+}$ or NP$_{(396–404)}{}^{+}$ CD8^{+} T cells in spleens 15 dpi with LCMV Cl13 following *in vivo* ligation of PSGL-1 or isotype control antibody.
(I and J) TCF-1 and TOX expression in CD44^{hi} donor OT-I cells in tumors and inguinal tumor DLNs of WT mice inoculated with B16-OVA melanoma cells. Donor cells were *in vitro* activated, transferred on day 14 of tumor growth, and analyzed 6 days later.
(A–J) Each dot represents a biological replicate. Data are parametric except those noted by a hash symbol (#). For parametric data, unpaired t tests were performed; Mann-Whitney test used for non-parametric data. Error bars are SEM. The experiment was performed 1× (B, TOX; E–G), 2× (A and B, TCF-1; H–J), or 33 (C and D).
See also Figure S6.

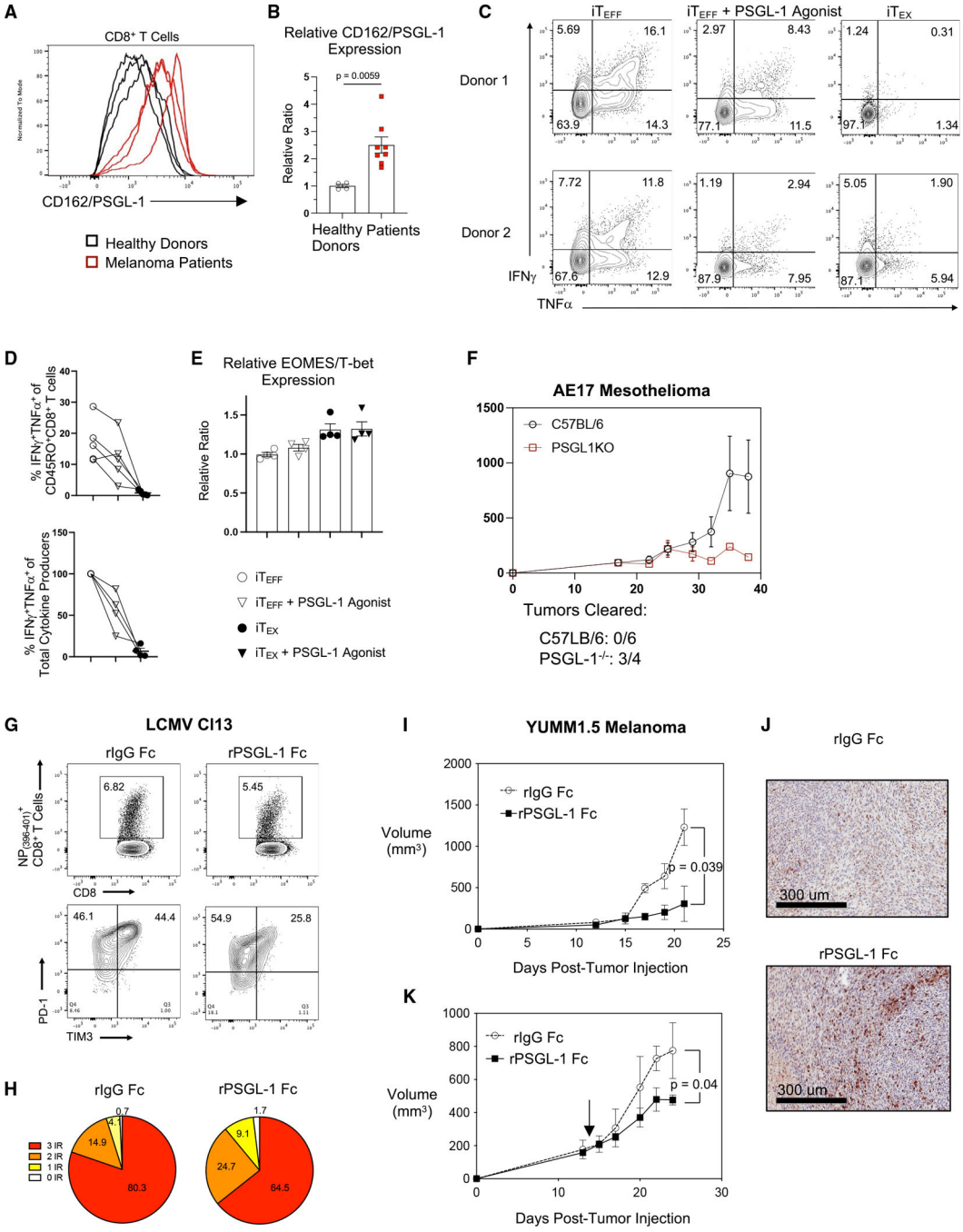

Figure 7. Pharmacological inhibition of PSGL-1 promotes decreased T cell exhaustion and functional T cell responses

(A) Histograms of CD162/PSGL-1 expression on activated CD8$^+$ T cells from 3 healthy donors and 3 patients with melanoma.

(B) Relative expression of PSGL-1 on CD8$^+$ T cells from healthy donors and patients with melanoma.

(C–E) PBMCs from healthy donors were assessed for transcription factor expression or restimulated to assess cytokine production.

(C) Flow cytometry plots showing IFNγ and TNF-α production by $CD8^+$ T cells from two different healthy donor PBMCs after iT_{EFF} or iT_{EX} culture and restimulated on day 9; pre-gated on live, $CD8^+CD45RO^+$ cells.

(D) Top: frequencies of IFNγ and TNF-α double-producing $CD8^+CD45RO^+$ cells cultured under iT_{EFF}, iT_{EFF} + PSGL-1 agonist, or iT_{EX} conditions. Lines are connecting data from the same donor under the different culture conditions. Bottom: relative reduction of IFNγ and TNF-α double-producing $CD8^+CD45RO^+$ cells upon PSGL-1 ligation under iT_{EFF} conditions (4 out of 5 donors).

(E) EOMES/T-bet expression ratio in $CD8^+CD45RO^+$ cells from donors in (D).

(A–E) Each dot represents a unique donor. Experiments were performed 2× (A and B) or 3× (C–E). Data are parametric data; unpaired t tests were performed. Error bars are SEM.

(F) Growth (volume) of AE17 mesothelioma tumors in C57BL/6 and PSGL-$1^{-/-}$ mice.

(G) Top: splenic $NP_{(396–404)}$-specific $CD8^+$ T cells of control- and recombinant PSGL-1-human Fc protein (rPSGL-1 Fc)-treated LCMV Cl13-infected mice assessed on 8 dpi. Bottom: PD-1 and TIM-3 expression on $NP_{(396–404)}$-specific $CD8^+$ T cells.

(H) Co-expression of PD-1, LAG3, and TIM-3 on $NP_{(396–404)}$ specific $CD8^+$ T cells assessed via Boolean gating.

(I) Growth of YUMM1.5 tumors in control C57BL/6 mice and mice treated with rPSGL-1 Fc beginning on day 0.

(J) Representative H&E histology with anti-CD3 staining of YUMM1.5 tumor sections collected on day 21. (K) YUMM1.5 tumor volumes following therapeutic treatment with rPSGL-1 Fc beginning on day 14.

(F–J) Experiments were performed 2× with >3 mice/group per experiment.

See also Figure S7.

KEY RESOURCES TABLE

REAGENT or RESOURCE	SOURCE	IDENTIFIER
Antibodies		
BUV395 Mouse Anti-Human CD4	BD Biosciences	Cat# 563550; RRID: AB_2738273
BUV395 Rat Anti-Mouse CD8a	BD Biosciences	Cat# 563786; RRID: AB_2732919
BUV496 Mouse Anti-Human CD8	BD Biosciences	Cat# 612942; RRID: AB_2870223
BUV737 Mouse Anti-Human CD45RA	BD Biosciences	Cat# 612846; RRID: AB_2870168
BUV737 Mouse Anti-Mouse CD45.1	BD Biosciences	Cat# 612811; RRID: AB_2870136
BUV737 Rat Anti-Mouse CD11a	BD Biosciences	Cat# 741727; RRID: AB_2871097
BUV737 Rat Anti-Mouse CD223	BD Biosciences	Cat# 741820; RRID: AB_2871155
BV421 Mouse Anti-Mouse CD244.2	BD Biosciences	Cat# 740015; RRID: AB_2739787
BV421 Rat Anti-Mouse CD244.1	BD Biosciences	Cat# 744284; RRID: AB_2871568
BV480 Mouse Anti-Human CD44	BD Biosciences	Cat# 746479; RRID: AB_2743781
BV605 Mouse Anti-Mouse Ly-108	BD Biosciences	Cat# 745250; RRID: AB_2742834
R718 Rat Anti-Human CCR7 (CD197)	BD Biosciences	Cat# 751861
R718 Rat Anti-Mouse CD4	BD Biosciences	Cat# 566939; RRID: AB_2869957
Alexa Fluor® 647 anti-human CD101 (BB27)	BioLegend	Cat# 331010; RRID: 2562145
APC/Fire™ 750 anti-human CD45RO	BioLegend	Cat# 304250; RRID: AB_2616717
APC/Fire™ 750 anti-mouse CD38	BioLegend	Cat# 102738; RRID: AB_2876402
Apotracker™ Green	BioLegend	Cat# 427403
Brilliant Violet 421™ anti-human CD38	BioLegend	Cat# 303526; RRID: AB_10900230
Brilliant Violet 605™ anti-human CD25	BioLegend	Cat# 302632; RRID: AB_11218989
Brilliant Violet 605™ anti-rat CD90/mouse CD90.1 (Thy-1.1)	BioLegend	Cat# 202537; RRID: AB_2562644
Brilliant Violet 711™ anti-human CD366 (Tim-3)	BioLegend	Cat# 345024; RRID: AB_2564046
Brilliant Violet 711™ anti-mouse CD366 (Tim-3)	BioLegend	Cat# 119727; RRID: AB_2716208
Brilliant Violet 785™ anti-human CD223 (LAG-3)	BioLegend	Cat# 369322; RRID: AB_2716127
Brilliant Violet 785™ anti-mouse CD279 (PD-1)	BioLegend	Cat# 135225; RRID: AB_2563680
PE/Cyanine7 anti-mouse CD25	BioLegend	Cat# 101916; RRID: AB_2616762
APC anti-mouse CD69	BioLegend	Cat# 104514; RRID: AB_492843
BUV496 Rat Anti-Mouse CD44	BD Bioscience	Cat# 741057; RRID: AB_2870671
Brilliant Violet 421™ anti-mouse CX3CR1	BioLegend	Cat# 149023; RRID: AB_2565706
FITC anti-mouse CD45.1	BioLegend	Cat# 110706; RRID: AB_313495
FITC anti-mouse CD49d	BioLegend	Cat# 103606; RRID: AB_313037
Human TruStain FcX™	BioLegend	Cat# 422302; RRID: AB_2818986
PE anti-human CD39	BioLegend	Cat# 328208; RRID: AB_940429
PE anti-mouse CD160	BioLegend	Cat# 143004; RRID: AB_10960743
PE/Cyanine7 anti-human CD160	BioLegend	Cat# 341212; RRID: AB_2562876
PE/Dazzle™ 594 anti-human CD279 (PD-1)	BioLegend	Cat# 367434; RRID: AB_2783284
PE/Dazzle™ 594 anti-mouse CD62L	BioLegend	Cat# 104448; RRID: AB_2566163
PE/Dazzle™ 594 anti-mouse CD90.2 (Thy-1.2)	BioLegend	Cat# 140329; RRID: AB_2650965

REAGENT or RESOURCE	SOURCE	IDENTIFIER
PerCP/Cyanine5.5 anti-human CD69	BioLegend	Cat# 310926; RRID: AB_2074956
PerCP/Cyanine5.5 anti-mouse CD107a (LAMP-1)	BioLegend	Cat# 121626; RRID: AB_2572055
PerCP/Cyanine5.5 anti-mouse CD223 (LAG-3)	BioLegend	Cat# 125212; RRID: AB_2561517
Purified anti-mouse CD16/32	BioLegend	Cat# 101302; AB_312801
CD101 PECy7	eBioscience/ThermoFisher	Cat# 25–1011-82; RRID: AB_2573378
H2-D(b) GP(33–41) APC or BV421 Tetramer	NIH Tetramer Core	N/A
H2-D(b) NP(396–401) BV421 Tetramer	NIH Tetramer Core	N/A
PE Mouse Anti-TCF-7/TCF-1	BD Biosciences	Cat# 564217; RRID: AB_2687845
PE Mouse Anti-TCF-7/TCF-1	BD Biosciences	564217
APC anti-human TNF-α	BioLegend	Cat# 502912; RRID: AB_315264
APC anti-mouse IFN-γ	BioLegend	Cat# 505810; RRID: AB_315404
APC anti-mouse Perforin	BioLegend	Cat# 154304; RRID: AB_2721463
Brilliant Violet 421™ anti-human IFN-γ	BioLegend	Cat# 502532; RRID: AB_2561398
Brilliant Violet 421™ anti-human/mouse Granzyme B	BioLegend	Cat# 396414; RRID: AB_2810603
Brilliant Violet 421™ anti-T-bet	BioLegend	Cat# 644816; RRID: AB_10959653
PE anti-human IL-2	BioLegend	Cat# 500307; RRID: AB_315094
PE anti-mouse IL-2	BioLegend	Cat# 503808; RRID: AB_315302
PE/Cyanine7 anti-mouse TNF-α	BioLegend	Cat# 506324; RRID: AB_2256076
Alexa Fluor 647 Mouse Anti-ZAP70	BioLegend	Cat# 691205; RRID: AB_2721438
Brilliant Violet 421™ anti-Mouse CD3	BioLegend	Cat# 100228; RRID: AB_2562553
CD162 (PSGL-1) PE	eBioscience/ThermoFisher	Cat# 12–1621-82; RRID: AB_2848256
EOMES PECy7	eBioscience/ThermoFisher	Cat# 25–4875-82; AB_2573454
EOMES PerCP-eFluor710	eBioscience/ThermoFisher	Cat# 46–4877-42; RRID: AB_2573759
Ki67 PerCP-eFluor710	eBioscience/ThermoFisher	Cat# 46–5698-82; RRID: AB_11040981
T-bet eFluor 450	eBioscience/ThermoFisher	Cat# 48–5825-82; RRID: AB_2784727
TOX eFluor 660	eBioscience/ThermoFisher	Cat# 50–6502-82; RRID: AB_2574265
UBASH3B/STS 1 polyclonal Rabbit IgG antibody	Proteintech	Cat# 19563–1-AP; RRID: AB_10643379
B-actin Mouse mAb	Cell Signaling	Cat# 3700; RRID: AB_2242334
IRDye800CW Goat anti-Rabbit IgG Secondary Antibody	Licor	Cat# 926–32211; RRID: AB_621843
IRDye680RD Goat anti-Mouse IgG Secondary Antibody	Licor	Cat# 926–68070; RRID: AB_10956588
Zap70 Rabbit mAb	Cell Signaling	Cat# 2705; RRID: AB_2273231
Phospho-Zap-70 (Tyr319)/Syk (Tyr352) Rabbit mAb	Cell Signaling	Cat# 2717; RRID: AB_2218658
Akt (pan) Mouse mAb	Cell Signaling	Cat# 2920; RRID: AB_1147620
Phospho-Akt (Ser473) Rabbit mAb	Cell Signaling	Cat# 9271; RRID: AB_329825
p44/42 MAPK (Erk1/2) Mouse mAb	Cell Signaling	Cat# 4696; RRID: AB_390780
Phospho-p44/42 MAPK (Erk1/2) (Thr202/Thyr204) XP Rabbit mAb	Cell Signaling	Cat# 4370; RRID: AB_2315112
Fab anti-mouse CD162 (PSGL-1)	mAb from BioXcell, Fab fragments custom made by Ab Lab (University of Vancourer, BC)	mAb: Cat# BE0186; RRID: AB_10950305
Anti-mouse CD3e	BioXCell	Cat# BE0001–1; RRID: AB_1107634
Anti-mouse CD28	BioXCell	Cat# BE00015–1

REAGENT or RESOURCE	SOURCE	IDENTIFIER
ImmunoCult Human CD3/CD28 T Cell Activator	StemCell	Cat# 10971
Bacterial and virus strains		
LCMV Clone 13	This lab	N/A
Biological samples		
Human PBMCs, melanoma patients	University of California San Diego, Moore's Cancer Center	N/A
Human PBMCs, healthy controls	iXCells	10HU-003-CR50M
Chemicals, peptides, and recombinant proteins		
SIINFEKL (OVA, N4)	GenScript, Custom Order	N/A
SIIQFEKL (OVA, Q4)	GenScript, Custom Order	N/A
SIITFEKL (OVA, T4)	GenScript, Custom Order	N/A
SIIVFELK (OVA, V4)	GenScript, Custom Order	N/A
REAGENT or RESOURCE	SOURCE	IDENTIFIER
KAVYNFATM (LCMV GP33–41)	GenScript, Custom Order	N/A
FQPQNGQFI (LCMV NP396–404)	GenScript, Custom Order	N/A
Recombinant PSGL-1	This lab, Aragen Life Sciences	N/A
Critical commercial assays		
eBioscience Foxp3/Transcription Factor Staining Buffer Set	ThermoFisher	00–5523-00
2-NBDG	Cayman Chemical	11046
Miltenyi Mouse Tumor Dissociation Kit	Miltenyi Biotec	130–096-730
APEX AF488 Microscale Protein Labeling Kit	ThermoFisher	A30006
Seahorse Glycolytic Rate Assays	Agilent Technologies	103346–100
10X Single Cell 3' Reagent Kits v2	10X Genomics	Multiple
Deposited data		
WT vs PSGL-1$^{-/-}$ CD8^{+} T cells, LCMV Cl13	Reference #6 (Tinoco)	GEO: GSE80113
Epigenetics of CD8^{+} T cells during differentiation	Reference #59 (Yu)	GEO: GSE89036
Raw and analyzed scRNA-seq data	This paper	GEO: GSE226523
Raw and analyzed ATAC-seq data	This paper	GEO: GSE226521
Experimental models: Cell lines		
YUMM1.5 melanoma	Marcus Bosenburg	N/A
B16-OVA melanoma	Ananda Goldrath	N/A
TK-1 T cell lymphoblast	ATCC	CRL-2396
Experimental models: Organisms/strains		
C57BL/6J	The Jackson Laboratory	000664
B6.Cg-*Selplg*^{tm1Fur}/J (PSGL-1$^{-/-}$)	The Jackson Laboratory	004201

REAGENT or RESOURCE	SOURCE	IDENTIFIER
C57BL/6 Tg(TcraTcrb)1100Mjb/J (OT-I)	The Jackson Laboratory	003831
B6.Cg-*Tcra*^{tm1Mom}Tg(TcrLCMV)327Sdz/TacMmjax (P14)	The Jackson Laboratory	025408
B6.SJL-*Ptprc*^{a}*Pepc*^{b}/BoyJ (CD45.1)	The Jackson Laboratory	000686
B6.PL-*Thy1*^{a}/CyJ (CD90.1/Thy1.1)	The Jackson Laboratory	000406
Software and algorithms		
FlowJo v10	FlowJo, BD	N/A
INSPIRE V200.1.388.0	Amnis	N/A
IDEAS V6.2.183.0	Amnis	N/A
SeqGeq	FlowJo, BD	N/A
WAVE	Agilent Technologies	N/A
GraphPad Prism 9	GraphPad	N/A
MSstats TMT Bioconductor	Bioconductor	N/A
IntegrateData	Seurat V4.1.1.	N/A
RunUMAP	Seurat V4.1.1.	N/A
FindClusters	Seurat V4.1.1.	N/A
FindAllMarkers	Seurat V4.1.1.	N/A
DoHeatmap	Seurat V4.1.1.	N/A
VlnPlot	Seurat V4.1.1.	N/A
Stat_compare_means	ggpubr V0.4.0.	N/A
IGV Genome Browser V2.9.2.	Broad Institute	N/A
IPA Pathway Analysis	Qiagen	N/A
10X Genomics Cell Ranger V2.2.0.	10X Genomics	N/A
MaxQuant Software 1.6.11.0	MaxQuant	N/A